

## Assessing the relationship between microwave vegetation optical depth and gross primary production

Irene E. Teubner<sup>a,\*</sup>, Matthias Forkel<sup>a</sup>, Martin Jung<sup>b</sup>, Yi Y. Liu<sup>c</sup>, Diego G. Miralles<sup>d</sup>, Robert Parinussa<sup>e</sup>, Robin van der Schalie<sup>e</sup>, Mariette Vreugdenhil<sup>a</sup>, Christopher R. Schwalm<sup>f,g</sup>, Gianluca Tramontana<sup>h</sup>, Gustau Camps-Valls<sup>i</sup>, Wouter A. Dorigo<sup>a</sup>

<sup>a</sup> Department of Geodesy and Geoinformation, TU Wien, Gußhausstraße 27-29, 1040 Vienna, Austria

<sup>b</sup> Department for Biogeochemical Integration, Max Planck Institute for Biogeochemistry, P.O. Box 10 01 64, 07701 Jena, Germany

<sup>c</sup> School of Geography and Remote Sensing, Nanjing University of Information Science & Technology (NUIST), No.219, Ningliu Road, Nanjing, Jiangsu 210044, China

<sup>d</sup> Laboratory of Hydrology and Water Management, Ghent University, Campus Coupure, Coupure links 653, B-9000 Ghent, Belgium

<sup>e</sup> VanderSat B.V., Huygensstraat 34, 2201 DK Noordwijk, The Netherlands

<sup>f</sup> Woods Hole Research Center, 149 Woods Hole Road, Falmouth, MA 02540-1644, USA

<sup>g</sup> Center for Ecosystem Science and Society, Northern Arizona University, P.O. Box 5620, Flagstaff, AZ 86011, USA

<sup>h</sup> Department for Innovation in Biological Agro-food and Forest systems (DIBAF), Tuscia University, Via San Camillo de Lellis s.n.c., 01100 Viterbo, Italy

<sup>i</sup> Image and Signal Processing Group (ISP), Universitat de València, Calle Catedrático José Beltrán 2, 46980 Paterna (València), Spain

### ARTICLE INFO

#### Keywords:

Microwave remote sensing  
Vegetation dynamics  
Ecosystem productivity  
ASCAT  
SMOS  
AMSR-E

### ABSTRACT

At the global scale, the uptake of atmospheric carbon dioxide by terrestrial ecosystems through photosynthesis is commonly estimated through vegetation indices or biophysical properties derived from optical remote sensing data. Microwave observations of vegetated areas are sensitive to different components of the vegetation layer than observations in the optical domain and may therefore provide complementary information on the vegetation state, which may be used in the estimation of Gross Primary Production (GPP). However, the relation between GPP and Vegetation Optical Depth (VOD), a biophysical quantity derived from microwave observations, is not yet known. This study aims to explore the relationship between VOD and GPP. VOD data were taken from different frequencies (L-, C-, and X-band) and from both active and passive microwave sensors, including the Advanced Scatterometer (ASCAT), the Soil Moisture Ocean Salinity (SMOS) mission, the Advanced Microwave Scanning Radiometer for Earth Observation System (AMSR-E) and a merged VOD data set from various passive microwave sensors. VOD data were compared against FLUXCOM GPP and Solar-Induced chlorophyll Fluorescence (SIF) from the Global Ozone Monitoring Experiment-2 (GOME-2). FLUXCOM GPP estimates are based on the upscaling of flux tower GPP observations using optical satellite data, while SIF observations present a measure of photosynthetic activity and are often used as a proxy for GPP. For relating VOD to GPP, three variables were analyzed: original VOD time series, temporal changes in VOD ( $\Delta\text{VOD}$ ), and positive changes in VOD ( $\Delta\text{VOD}_{\geq 0}$ ). Results show widespread positive correlations between VOD and GPP with some negative correlations mainly occurring in dry and wet regions for active and passive VOD, respectively. Correlations between VOD and GPP were similar or higher than between VOD and SIF. When comparing the three variables for relating VOD to GPP, correlations with GPP were higher for the original VOD time series than for  $\Delta\text{VOD}$  or  $\Delta\text{VOD}_{\geq 0}$  in case of sparsely to moderately vegetated areas and evergreen forests, while the opposite was true for deciduous forests. Results suggest that original VOD time series should be used jointly with changes in VOD for the estimation of GPP across biomes, which may further benefit from combining active and passive VOD data.

\* Corresponding author.

E-mail addresses: [irene.teubner@geo.tuwien.ac.at](mailto:irene.teubner@geo.tuwien.ac.at) (I.E. Teubner), [matthias.forkel@geo.tuwien.ac.at](mailto:matthias.forkel@geo.tuwien.ac.at) (M. Forkel), [mjung@bgc-jena.mpg.de](mailto:mjung@bgc-jena.mpg.de) (M. Jung), [yiliu001@gmail.com](mailto:yiliu001@gmail.com) (Y.Y. Liu), [diego.miralles@UGent.be](mailto:diego.miralles@UGent.be) (D.G. Miralles), [rparinussa@vandersat.com](mailto:rparinussa@vandersat.com) (R. Parinussa), [rvanderschalie@vandersat.com](mailto:rvanderschalie@vandersat.com) (R. van der Schalie), [Mariette.Vreugdenhil@geo.tuwien.ac.at](mailto:Mariette.Vreugdenhil@geo.tuwien.ac.at) (M. Vreugdenhil), [cschwalm@whrc.org](mailto:cschwalm@whrc.org) (C.R. Schwalm), [g.tramontana@unitus.it](mailto:g.tramontana@unitus.it) (G. Tramontana), [gcamps@uv.es](mailto:gcamps@uv.es) (G. Camps-Valls), [Wouter.Dorigo@geo.tuwien.ac.at](mailto:Wouter.Dorigo@geo.tuwien.ac.at) (W.A. Dorigo).

<http://dx.doi.org/10.1016/j.jag.2017.10.006>

Received 4 July 2017; Received in revised form 14 October 2017; Accepted 17 October 2017

Available online 05 November 2017

0303-2434/ © 2017 Elsevier B.V. All rights reserved.

## 1. Introduction

Vegetation plays an important role in the Earth system as plants take up atmospheric carbon dioxide through photosynthesis and transport water from the soil into the atmosphere through transpiration (Lambers et al., 2008). In addition, vegetation can influence the Earth's surface energy balance through differences in surface albedo compared to bare soil or snow cover, which is especially pronounced for boreal forests (Bonan, 2008). Therefore, monitoring the vegetation state in terms of photosynthetic activity as well as plant water status is of importance for hydrological, ecological and climate change applications (Bonan, 2015).

The uptake of atmospheric carbon dioxide by vegetation through photosynthesis is commonly referred to as Gross Primary Production (GPP) and is the largest carbon flux in the global carbon cycle (Ciais et al., 2013). GPP can be determined at site level from eddy covariance measurements of carbon dioxide net exchange, which is partitioned into GPP and ecosystem respiration (Baldocchi et al., 2001; Reichstein et al., 2005; Jung et al., 2011; Lasslop et al., 2012). Another approach is the biometric method, which combines estimates of plant growth, chamber flux measurements and stock inventories (Campioli et al., 2016). GPP can be assessed from local to global scales using process-based models that describe the canopy light absorption and the energy and enzyme limitations of the carboxylation rate to estimate gross carbon assimilation (e.g. Farquhar et al., 1980; Collatz et al., 1992). However, current process-based models show large uncertainties because of a limited understanding of the processes that are involved in photosynthesis (Rogers et al., 2017). Alternatively, data-driven approaches that combine satellite observations with empirical models can be used to estimate GPP at large scales (Beer et al., 2010).

Most of the approaches to estimate GPP from satellite observations use optical data to characterize biophysical properties or photosynthetic activity. Biophysical properties such as the Fraction of Absorbed Photosynthetically Active Radiation (FAPAR) are used in light-use efficiency models to estimate GPP, assuming a linear relationship between FAPAR and GPP which is modulated by temperature and water stress (Monteith, 1972; Nemani et al., 2003). Additionally, machine learning algorithms, driven by meteorological and/or satellite data, have been used to upscale site-level observations of GPP (Beer et al., 2010; Jung et al., 2011; Tramontana et al., 2016). Alternatively, Solar-Induced chlorophyll Fluorescence (SIF), an estimate of photosynthetic activity, has been proposed as a global proxy for GPP in recent years (Frankenberg et al., 2014; Guanter et al., 2014; Damm et al., 2015; Zhang et al., 2016).

Optical remote sensing data, however, are often affected by clouds and aerosols (Myneni et al., 2002; Forkel et al., 2013) and sun-sensor geometry (Dorigo, 2012; Morton et al., 2014). A common method to reduce the influence of cloud cover on optical data is temporal compositing (Huete et al., 2011; Holben, 1986), which decreases the native temporal resolution. Alternatively, time series filtering can be applied (Chen et al., 2004).

In contrast to optical data, microwave radiation below a frequency of 10 GHz is less influenced by clouds and is independent of the sun as source of illumination (Woodhouse, 2005). Microwave satellite observations over vegetation are thus able to provide crucial information in areas with extensive cloud cover like the tropics or high latitudes. The penetration depth of the microwave radiation into the vegetation canopy depends on frequency, dielectric properties, size and geometry of the interacting vegetation parts. As such, microwave observations from different frequencies theoretically contain information from different parts of the vegetation (Woodhouse, 2005). Whereas high frequencies (short wavelengths) predominantly interact with small structures like leaves and twigs at the top of the vegetation layer, low frequencies (long wavelengths) can penetrate deeper into the vegetation and are more sensitive to large structures like branches or trunks (Woodhouse, 2005). Accordingly, microwave radiation exhibits a

higher penetration depth than optical radiation due to its longer wavelength, and should theoretically be better suited for monitoring denser canopies, as the observed signal does not saturate as quickly as for optical sensors (Woodhouse, 2005; Dorigo et al., 2007). Therefore, microwave satellite observations have the potential to provide valuable information on the vegetation state complementary to optical satellite data which are traditionally used for estimating GPP.

Microwave Vegetation Optical Depth (VOD) describes the attenuation of radiation due to scattering and absorption within the vegetation layer, which is caused by the water contained in the vegetation (Woodhouse, 2005). At low biomass, VOD is linearly related to the vegetation water content (VWC; expressed in kg/m<sup>2</sup>) (Jackson and Schmugge, 1991; Woodhouse, 2005). In addition, VOD can be related to aboveground living biomass (Liu et al., 2015; Tian et al., 2016) and to Leaf Area Index (LAI), especially in crop- and grasslands (Zribi et al., 2011; Kim et al., 2012; Sawada et al., 2016).

VOD data have been analyzed for different applications such as long-term trends in biomass (Andela et al., 2013; Liu et al., 2013a,b, 2015), forest loss (Marle et al., 2016), phenology metrics (Jones et al., 2011, 2012), vegetation water stress (Miralles et al., 2016), evaporation retrievals (Miralles et al., 2011; Martens et al., 2016) and ecosystem resilience (Verbesselt et al., 2016). However, short-term variations in VOD have not been assessed with regard to GPP.

The aim of this study is to explore the relationship between VOD and GPP and assess if VOD can provide additional information about GPP on top of what is provided by SIF. In addition, this study investigates the effect of different microwave frequencies (between 1 and 10 GHz) and of active and passive sensors (hereafter referred to as active and passive VOD) on the relationship between VOD and GPP.

## 2. Data and methods

### 2.1. Vegetation remote sensing data

The analysis is based on five VOD data sets, upscaled GPP estimates, and SIF observations (Table 1). The data sets have different temporal coverage with a common overlap of about one year. The period from January 2007 to December 2015 was selected in order to obtain a minimum number of four years of overlap with the GPP data set.

#### 2.1.1. VOD ASCAT

Active microwave VOD data were retrieved from microwave backscatter measurements of the Advanced Scatterometer (ASCAT) onboard the meteorological operational satellite A (MetOp-A). ASCAT measures backscatter at 5.25 GHz (C-band) in vertical co-polarization. The retrieval of VOD is based on slope estimates of the angular backscatter dependency, which are calculated during the soil moisture retrieval using the TU-Wien change detection algorithm. VOD is obtained by relating the angular sensitivity of measured backscatter to the sensitivity of modelled bare soil backscatter (Melzer, 2013; Vreugdenhil et al., 2016a,b) and, therefore, represents a measure of volume scattering due to vegetation relative to bare soil volume scattering. VOD is derived jointly from measurements in ascending and descending mode (9:30 a.m./p.m. equatorial crossing).

#### 2.1.2. VOD AMSR-E

Measurements at 6.9 GHz (C-band) and 10.7 GHz (X-band) were used from the Advanced Microwave Scanning Radiometer for Earth Observation System (AMSR-E). For both frequencies, VOD was obtained with the Land Parameter Retrieval Model (LPRM) v06 (van der Schalie et al., 2017). The algorithm uses a radiative transfer model (Mo et al., 1982) and includes an analytical solution for VOD using the Microwave Polarization Difference Index (MPDI) (Meesters et al., 2005). LPRM retrieves VOD and soil moisture simultaneously under the assumption of a globally constant single scattering albedo and further assumes that soil and canopy temperature are similar (Owe et al., 2001). Since the

**Table 1**  
Data set overview.

Name	Data set	Period used	Frequency/wavelength/data input	Spatial resolution	Temporal resolution	Type	Method/algorithm	Reference
SMOS	SMOS	7/2010–12/2015	1.4 GHz	0.25°	Daily	Passive microwave	LPRMv06	van der Schalie et al. (2017)
ASCAT	ASCAT	1/2007–12/2015	5.25 GHz	12.5 km	Daily	Active microwave	TU-Wien change detection	
AMSRE_C	AMSRE-E	1/2007–9/2011	6.9 GHz	0.25°	Daily	Passive microwave	LPRMv06	van der Schalie et al. (2017)
AMSRE_X	AMSRE-E	1/2007–9/2011	10.7 GHz	0.25°	Daily	Passive microwave	LPRMv06	van der Schalie et al. (2017)
VODmerged	AMSRE-E, WindSat, FY-3B	1/2007–9/2011, 1/2007–6/2012, 11/2010–12/2012	6.9 GHz, 6.8 GHz, 10.7 GHz	0.25°	Daily	Passive microwave	LPRMv05	Liu et al. (2015)
GPP	FLUXCOM	1/2007–12/2015	MODIS EVI, LAI, MIR, NDVI, NDWI	10 km	8-daily	Optical	Machine learning	Tramontana et al. (2016)
SIF	GOME2_F v26	1/2007–12/2015	740 nm	0.5°	Monthly	Optical		Joiner et al. (2013, 2014)

Acronyms: Enhanced Vegetation Index (EVI), Leaf Area Index (LAI), MODIS band 7 – Middle Infrared Reflectance (MIR), Normalized Difference Vegetation Index (NDVI), Normalized Difference Water Index (NDWI), and Land Parameter Retrieval Model (LPRM).

latter assumption generally does not hold for daytime observations, we only used observations from the descending mode for this analysis (1:30 a.m. equatorial crossing).

### 2.1.3. VOD SMOS

VOD from the Soil Moisture Ocean Salinity (SMOS) radiometer, which provides observations at 1.4 GHz (L-band), was also retrieved with the LPRM v06 (van der Schalie et al., 2016, 2017). Only data from the ascending mode were analyzed (6 a.m. equatorial crossing) as soil and canopy temperatures are usually more similar in the morning than in the late afternoon although seasonal and latitudinal variations exist.

### 2.1.4. VOD merged

In addition to the single frequency data sets, a merged passive microwave VOD data set developed by Liu et al. (2015) was included in this analysis. For the period 2007–2012, the data set comprises observations from AMSR-E (6.9 GHz, C-band), WindSat (6.8 GHz, C-band), and the FengYun-3B Microwave Radiometer Imager (10.7 GHz, X-band). Prior to merging, the single sensor data sets were rescaled by applying the cumulative distribution function (CDF) matching technique with AMSR-E as the reference (Liu et al., 2009).

### 2.1.5. GPP FLUXCOM

The FLUXCOM GPP data set presents an upscaling of flux tower measurements based on multiple machine learning algorithms and satellite data (Tramontana et al., 2016). Different remotely sensed data in the optical domain from the Moderate Resolution Imaging Spectroradiometer (MODIS) were used as input, including the Enhanced Vegetation Index (EVI), LAI, band 7 - Middle Infrared Reflectance (MIR), Normalized Difference Vegetation Index (NDVI), and Normalized Difference Water Index (NDWI) (Tramontana et al., 2016).

### 2.1.6. SIF GOME-2

The GOME-F v26 SIF data were obtained from the Global Ozone Monitoring Experiment-2 (GOME-2) sensor. The retrieval is based on the filling-in of Fraunhofer lines, which is caused by the chlorophyll fluorescence emitted from the Earth's surface (Joiner et al., 2013). The algorithm uses principal components analysis and radiative transfer theory to determine SIF at 740 nm (Joiner et al., 2013, 2014, 2016). In this study, SIF observations from the MetOp-A platform were used.

## 2.2. Ancillary data

### 2.2.1. CCI land cover

The European Space Agency (ESA) Climate Change Initiative (CCI) global land cover data set v1.6.1 was used for identifying homogenous grid cells and stratifying results according to land cover. The data set is derived from Medium Resolution Imaging Spectrometer (MERIS) surface reflectance time series and has a spatial resolution of 300 m (Bontemps et al., 2013). The maps are available for three epochs that cover the periods 1998–2002, 2003–2007, and 2008–2012, respectively. In this study, the map for the period 2008–2012 was used as it falls within the overall data period.

### 2.2.2. GPCP

Precipitation data from the Global Precipitation Climatology Project (GPCP) are displayed as reference in the time series plot. GPCP 1DD version 1.2 provides daily precipitation estimates at 1° spatial resolution (Huffman et al., 2001). The precipitation estimates are produced from satellite data in the high frequency microwave (> 10 GHz) to infrared region in combination with gauge data (Huffman et al., 2001).

### 2.2.3. ERA-Interim

Skin temperature and snow depth from ERA-Interim were used to mask VOD. ERA-Interim is the current global atmospheric reanalysis produced by the European Centre for Medium-Range Weather Forecasts

for the period from 1979 onwards (Dee et al., 2011). Data are assimilated using a 4-dimensional variational analysis. The horizontal resolution is about 0.7° at the equator.

#### 2.2.4. Topographic complexity

Topographic complexity was used to mask VOD during the analysis of homogeneous grid cells. It is described by the standard deviation of elevation within a grid cell. A map of topographic complexity is available as ancillary data for the ESA-CCI soil moisture v02.2 data set (Dorigo et al., 2015) with a spatial resolution of 0.25°. The topographic complexity is computed from the USGS 30-Arc-Second Global Elevation Data Set (GTOPO30) (USGS, 1996).

#### 2.3. Variables for relating VOD to GPP

In this study, three variables for comparing VOD with GPP are investigated: (1) original time series of VOD, (2) change in VOD ( $\Delta\text{VOD}$ ), and (3) positive changes in VOD ( $\Delta\text{VOD}_{\geq 0}$ ). The latter two variables treat VOD as a proxy for aboveground biomass of the vegetation layer, which includes leaves and woody components. Liu et al. (2015) showed that the relationship between VOD and forest biomass data is monotonically increasing, which makes VOD a suitable proxy for biomass. Changes in VOD may thus relate to changes in biomass and hence to Aboveground Net Primary Production (ANPP), which contributes to total Net Primary Production (NPP).

- (1) Original VOD time series: For crop- and grasslands, VOD is proportional to total VWC (Jackson and Schmugge, 1991; Woodhouse, 2005) and thus scales with LAI (Zribi et al., 2011; Kim et al., 2012; Sawada et al., 2016), which in turn is related to GPP (Suyker et al., 2005; Gitelson et al., 2014). The original time series of VOD may thus be related to GPP.
- (2)  $\Delta\text{VOD}$ : For forests, ANPP is commonly estimated through biomass changes between two consecutive measurements (Clark et al., 2001a; Campioli et al., 2011, 2016; Nunes et al., 2013; Wagner et al., 2013a). Therein, biomass changes are determined from changes in stem circumference, which are converted to whole-tree biomass using allometric relations, and from litter traps or LAI. In this study, this method is adopted by calculating the change in VOD.

$$\Delta\text{VOD}(t) = \text{VOD}_t - \text{VOD}_{t-1}$$

where  $\Delta\text{VOD}(t)$  is the change in VOD at time  $t$ , and  $\text{VOD}_t$  and  $\text{VOD}_{t-1}$  are VOD observations at time  $t$  and  $t - 1$ , respectively.

- (3)  $\Delta\text{VOD}_{\geq 0}$ : For grasslands, common metrics for determining annual ANPP include peak standing biomass, difference between maximum and minimum standing biomass, sum of positive biomass changes with negative values set to zero, and change in biomass (Scurlock et al., 2002). These metrics are designed for a low number of observations as the sampling of herbaceous vegetation is destructive and is often carried out once per growing season. Since the study focuses on the temporal agreement instead of annual metrics and the change in VOD is already analyzed as the second variable, the method of positive biomass changes is used as third variable.

$$\Delta\text{VOD}_{\geq 0}(t) = \begin{cases} \Delta\text{VOD}(t) & \text{if } \Delta\text{VOD}(t) \geq 0 \\ 0 & \text{otherwise} \end{cases}$$

In order to compare the results of all three variables, changes in VOD ( $\Delta\text{VOD}$  and  $\Delta\text{VOD}_{\geq 0}$ ) are also compared with the FLUXCOM GPP data set although, conceptually, they should relate more closely to NPP than GPP. However, direct measurements of large-scale NPP are not possible and, therefore, NPP is often derived from remote sensing-based GPP estimates using either a constant NPP:GPP ratio at annual time scales (Waring et al., 1998) or the difference between GPP and

autotrophic respiration at shorter time scales (Running et al., 2004; Zhao et al., 2005). For this reason, VOD variables in this study are related to GPP and not to NPP.

#### 2.4. Data preparation

The global data sets of VOD and GPP were resampled to a common resolution of 8 days and 0.25°. Resampling was performed by averaging over the 8-day period for VOD data sets or over the grid points within each 0.25° by 0.25° grid cell for GPP. Prior to the resampling of the daily VOD data sets, the data were masked for conditions of frozen soil or snow based on ERA-Interim. Observations were excluded if the daily mean skin temperature was  $\leq 0^\circ\text{C}$  or snow cover was present. For consistency with the VOD data sets, GPP and SIF were also masked accordingly. Passive microwave observations can be affected by radio frequency interference (RFI), which is caused by artificial sources of radiation and hence is not related to land surface properties (Li et al., 2004; Njoku et al., 2005). Therefore, passive VOD data were additionally masked for RFI. For ASCAT, negative values can occur due to a lower sensitivity of the modelled bare soil backscatter compared to the observed backscatter in the angular dependency (Vreugdenhil et al., 2016a). These negative values were not set to zero in order to avoid introducing a bias. For the comparison with SIF observations, GPP and VOD data sets were further resampled to monthly and 0.5° resolution using temporal and spatial means, respectively.

Land cover data were converted into fractional land cover at 0.25° (or 0.5°) resolution using the level 1 legend of the CCI classification scheme. The resulting map of dominant land cover at 0.25° resolution is displayed in Fig. S1. The corresponding abbreviations are summarized in Tables 2 and S1. For global correlation maps, grid cells with a dominant land cover class of permanent snow/ice or water were systematically excluded.

For stratifying the results according to land cover, only homogeneous grid cells were evaluated in order to minimize the influence of pixel heterogeneity. Using the ESA CCI land cover map, a grid cell was considered homogeneous if the fraction of dominant land cover within a 0.25° by 0.25° grid cell exceeded an arbitrary threshold of 75%. Additionally, grid cells were discarded if either topographic complexity or percentage of water bodies were higher than 10% following Draper et al. (2012) and Dorigo et al. (2015), since both factors have a strong impact on the emitted or reflected microwave signal (Owe et al., 2008).

Data smoothing was applied in two cases: (1) prior to calculating changes in VOD ( $\Delta\text{VOD}$  and  $\Delta\text{VOD}_{\geq 0}$ ) and (2) for visualization purposes in the time series plots. The smoothing was performed using a Savitzky–Golay filter of order three with a window size of 11 observations.

#### 2.5. Statistical analysis

Linear relationships were assessed using correlation analysis. Prior to the correlation analysis, the assumption of normality was tested following D'Agostino (1971) and D'Agostino and Pearson (1973). As not all grid cell data were normally distributed ( $p > 0.05$ ), the non-

**Table 2**  
CCI land cover abbreviations.

Abbreviation	CCI land cover class
CRO	Cropland, rainfed
EBF	Tree cover, broadleaved, evergreen, closed to open (> 15%)
DBF	Tree cover, broadleaved, deciduous, closed to open (> 15%)
ENF	Tree cover, needleleaved, evergreen, closed to open (> 15%)
DNF	Tree cover, needleleaved, deciduous, closed to open (> 15%)
SHR	Shrubland
GRA	Grassland
SPARSE	Sparse vegetation (tree, shrub, herbaceous cover) (< 15%)

parametric Spearman rank correlation was used instead of the parametric Pearson correlation. Due to this absence of normal distribution for some grid cell data, non-parametric measures were used when analyzing full-length time series data: the median for displaying the global distribution of the data sets and the coefficient of quartile variation (CQV, Kokoska and Zwillinger, 2000) for assessing signal variability. CQV is calculated using the 25th (Q1) and the 75th (Q3) percentile:

$$\text{CQV} = \frac{(Q3 - Q1)}{(Q3 + Q1)}$$

In addition to the zero-lagged correlation analysis, time lags for which the cross-correlations maximized were calculated as an additional measure to determine how well the signals match. Results for homogeneous grid cells are displayed as violin plots, which are similar to box plots but visualize the kernel estimation of the data distribution.

To compare the data sets independent of the strong seasonal signals that affect vegetation properties in many regions, anomalies relative to the mean seasonal cycle were calculated. The mean seasonal cycles were obtained from the 8-daily or monthly time series by averaging over each valid day in a year within the study period. Due to the relatively short data periods, no detrending was applied prior to calculating the mean seasonal cycles.

Residuals of the GPP-SIF relationship were analyzed to assess the potential use of VOD for estimating GPP. Residuals were calculated using a linear regression model following Guanter et al. (2014) and Damm et al. (2015). The regression models were evaluated for each grid cell separately with SIF as predictor variable. For grid cells with a significant regression ( $p < 0.05$ ), residuals were obtained as the difference between the observed and the SIF-based estimate of GPP.

In addition to temporal correlations, spatial correlations were calculated to assess the similarity between maps. Since the spatial data were not normally distributed ( $p > 0.05$ ), Spearman rank correlation was used.

### 3. Results

#### 3.1. Global patterns of VOD, GPP and SIF

Temporal median values of VOD, GPP and SIF reveal similar spatial patterns (Fig. 1a–g), although spatial coverage of SMOS is reduced due to RFI masking. The spatial agreement with GPP is highest for SIF ( $r = 0.87$ ), followed by the passive VOD data sets ( $0.73 < r < 0.79$ ) and is lowest for ASCAT ( $r = 0.47$ ). In general, regions of high VOD, i.e. high biomass, coincide with highly productive regions, which are primarily located in the tropics. In addition, high values are also found at high latitudes. In these regions, data masking due to low temperature and snow results in wintertime data gaps, which in turn increases temporal median values as they represent medians over the growing season only. Nevertheless, these relatively high values of productivity or VOD at high latitudes are mainly consistent across data sets.

Considering the absolute values of the VOD data, the data range differs between the data sets, which relates on the one hand to differences in the retrieval algorithm and version number and on the other hand to differences in sensor frequency. Since the focus of this study, however, is the temporal agreement between the data sets, differences in the absolute values were not further analyzed.

Global temporal correlations between the original VOD time series and GPP at lag zero reveal positive agreement across large areas (Fig. 2a–e). However, also some regions with negative correlations are observed. For ASCAT, negative correlations are found in Central America, South America, Africa and Southeast Asia. The passive VOD data sets show negative correlations mainly in South America (in particular in the Amazon) and Southeast Asia. Although the results for different passive VOD data sets are similar in most areas, deviations from this behavior are found for SMOS and the merged VOD. For SMOS,

negative correlations in central Africa coincide with those for ASCAT. For the merged VOD, predominantly positive correlations with GPP are observed in the Amazon, which contrasts with the negative values found for the other passive VOD data sets and may be related to differences in the algorithm version. Compared to the VOD data sets, the correlation between GPP and SIF (Fig. 2f) is positive everywhere and on average much stronger. Nevertheless, also regions with no significant correlations ( $p > 0.05$ ) occur, which are mainly located in the tropics and in Australia. In the tropics, both GPP and SIF exhibit low variability, while the opposite, i.e. high variability for both data sets, is found in Australia (Fig. S2).

Correlations between the anomalies of VOD and GPP (Fig. 3a–e) also exhibit predominantly positive correlations. On average, the correlations are lower in magnitude than for the original time series but also show a lower number of negative values. Regions with relatively high correlations for the anomalies coincide with regions of high temporal agreement for the original time series, while some regions with negative correlations for the original time series result in no significant correlations for the anomalies. Highest correlation coefficients are observed in Australia. The correlations for the anomalies of GPP and SIF (Fig. 3f) are of similar strength as the correlations between the anomalies of GPP and VOD.

#### 3.2. Temporal agreement with respect to SIF

The direct comparison of correlations between VOD and either GPP or SIF at homogeneous grid points (Fig. 4) shows that the temporal agreement between VOD and SIF is similar to that found between VOD and GPP. In most cases, however, the median correlation coefficient is lower for the correlation between VOD and SIF than between VOD and GPP. This is especially pronounced for sparsely vegetated grid cells, which are mostly located in Australia (see Fig. 1h).

In order to assess if VOD can provide additional information about GPP on top of that provided by SIF, VOD was correlated with the residuals of the GPP-SIF relationship (Fig. 5). The spatial maps reveal mainly positive correlations with negative correlations in the same areas as for the original time series but show a larger number of not significant correlations. In those areas where correlations are significant, VOD can explain variations in GPP that are not expressed through SIF using linear regression.

#### 3.3. Comparison of the three variables for relating VOD to GPP

For the comparison of the three variables with GPP, only grid cells that resulted in significant correlations for all three variables are shown in Fig. 6. For shrub-, crop-, grassland and sparse vegetation, all three variables yielded consistent, mainly positive correlations. Median values are generally lowest for the correlation between SMOS and GPP and appear to increase with sensor frequency. In most cases, the original VOD time series result in higher median correlations with GPP than the changes in VOD. Highest median correlations are observed for shrubland for both frequencies of AMSR-E. Comparing the changes in VOD, results show that  $\Delta\text{VOD}_{\geq 0}$  generally leads to higher correlations than  $\Delta\text{VOD}$ .

For forests, results are not as consistent as for the sparsely to moderately vegetated areas. Nevertheless, forests also show on average a lower magnitude of correlation between SMOS and GPP than for the remaining VOD data sets. Similar as for the sparsely to moderately vegetated areas, evergreen needleleaf forests exhibit generally higher correlations for the original VOD time series than for  $\Delta\text{VOD}$  and  $\Delta\text{VOD}_{\geq 0}$ . In contrast, deciduous forests mainly yield higher median correlations for  $\Delta\text{VOD}$  and  $\Delta\text{VOD}_{\geq 0}$  than for the original VOD time series. Evergreen broadleaf forests, which exhibit low signal variability (see Fig. S2) and a high number of negative correlations, do not show a consistent pattern for the three variables. Comparing only the changes in VOD for all forests, median correlations tend to be higher for  $\Delta\text{VOD}$

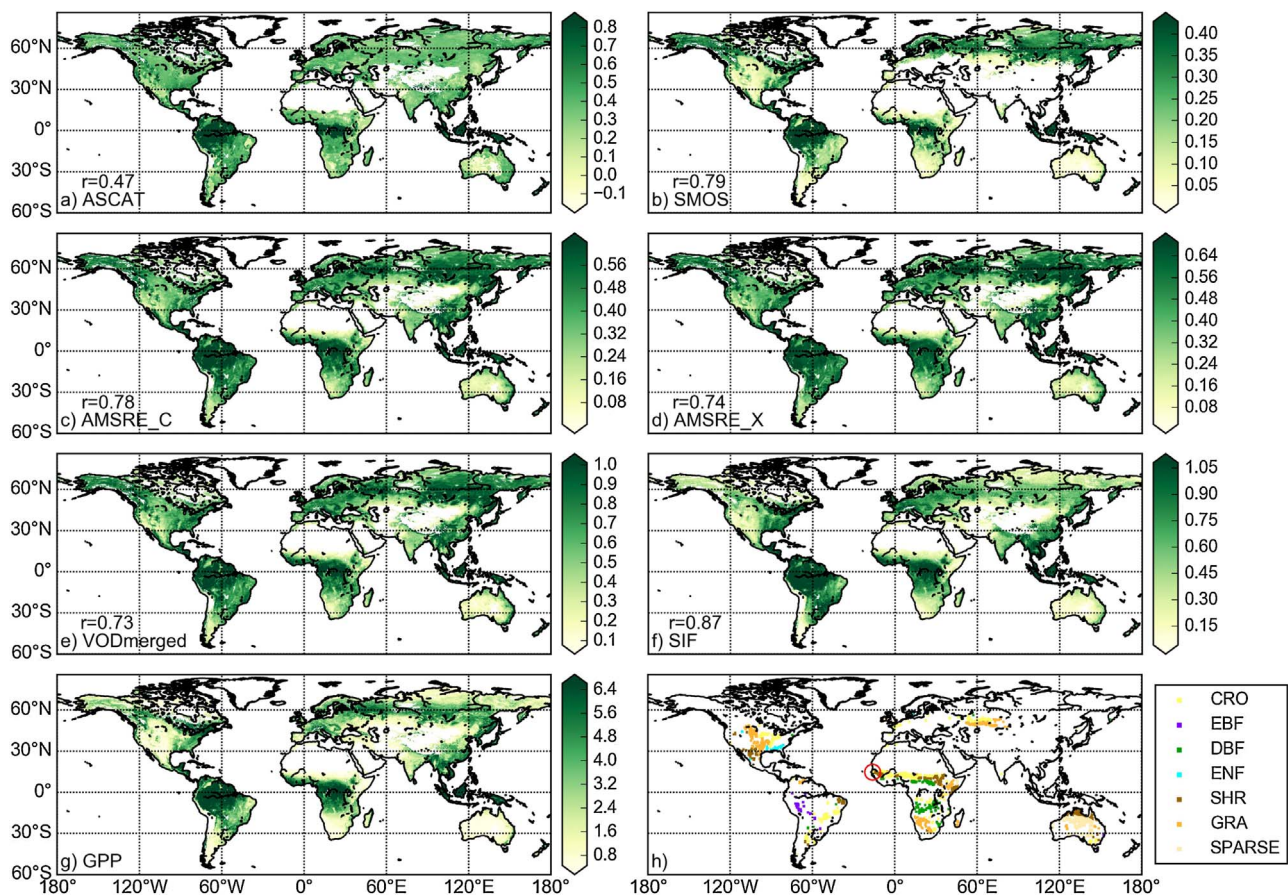


**Fig. 1.** (a–g) Temporal median value of VOD data sets (a–e), SIF (f) and GPP (g). VOD is dimensionless, GPP is in  $\text{gC m}^{-2} \text{d}^{-1}$  and SIF in  $\text{mW m}^{-2} \text{nm}^{-1} \text{sr}^{-1}$ . For visualization purposes, each data set is scaled between the 5th and the 95th percentile. (a–f)  $r$  denotes the spatial Spearman rank correlation between maps of temporal medians of GPP and VOD or SIF. All coefficients are highly significant ( $p < 0.001$ ). (h) Map of CCI land cover grid cells with a dominant land cover over 75% that correspond to the analyzed grid cells in Fig. 4. The center of the red circle marks the location of the grid cell shown in Fig. 8. Note that the size of the grid cells is enhanced for clearer visibility. (For interpretation of the references to color in this figure legend, the reader is referred to the web version of the article.)

than for  $\Delta\text{VOD}_{\geq 0}$  and thus show the opposite behavior as for the sparsely to moderately vegetated areas.

The spatial distributions of the correlations between GPP and the three VOD variables (Figs. 2, S6 and S7) tend to complement each other. For grid points where the original VOD time series results in high correlations,  $\Delta\text{VOD}$  and  $\Delta\text{VOD}_{\geq 0}$  have lower correlations and vice versa. Since  $\Delta\text{VOD}$  and  $\Delta\text{VOD}_{\geq 0}$  both represent changes in VOD, their spatial correlation patterns with GPP are more similar compared to the correlation pattern between original VOD time series and GPP (Table S2).

The lag analysis (Fig. 7) is based on the same grid cells as in Fig. 6. On average, the original VOD time series follow the GPP signal: changes in GPP are reflected with some delay by subsequent changes of the VOD signal. Apart from the broadleaf forests, all land cover classes exhibit median lag values ranging between 0 and 50 days. For ASCAT in deciduous broadleaf forest, the half a year's lag corresponds to the strong negative correlations found before for the zero-lagged correlations (Fig. 6). In contrast to the positive lag found for the original VOD time series, the lag values for  $\Delta\text{VOD}$  and  $\Delta\text{VOD}_{\geq 0}$  are negative, which indicates that changes in VOD generally precede the GPP signal. In some cases, as for example in the deciduous broadleaf forest for AMSRE\_C, AMSRE\_X and the merged VOD, the absolute value of the median lag is smaller for  $\Delta\text{VOD}$  and  $\Delta\text{VOD}_{\geq 0}$  than for the original VOD time series. In these cases, calculating the change in VOD leads to a closer temporal agreement with GPP, which corresponds to the higher correlation coefficients found for the zero-lagged correlations.

This shift from positive to negative lag values for the different variables is further illustrated in Fig. 8 for a rainfed cropland-

dominated grid cell. Comparing the data close to the seasonal peaks, the original VOD time series decrease slower than the GPP signal, resulting in a positive lag (Fig. 8b). For  $\Delta\text{VOD}$ , the signal rises earlier than for GPP, which yields a negative lag (Fig. 8c). Apart from the opposite sign of the lag value, the scaled  $\Delta\text{VOD}$  signal shows a different shape than the GPP signal.  $\Delta\text{VOD}$  exhibits a high number of values around 0.5, which represent  $\Delta\text{VOD}$  values close to zero and are a result of the relatively long period of small changes in VOD. In this case, considering only positive changes in VOD appears to result in a higher temporal matching with GPP (Fig. 8d), which explains the higher correlations found for  $\Delta\text{VOD}_{\geq 0}$  compared to  $\Delta\text{VOD}$  in sparsely to moderately vegetated areas (Fig. 6). Despite the overall higher temporal agreement for  $\Delta\text{VOD}_{\geq 0}$  than for  $\Delta\text{VOD}$ , the decline in GPP is better captured by  $\Delta\text{VOD}$ .

The relationships between the three VOD variables and GPP can be further assessed with the corresponding scatter plots (Fig. 8e–g). This relationship describes a seasonal hysteresis. Comparing all three variables, the shape of the mean seasonal cycle appears to be similar for the original VOD time series and  $\Delta\text{VOD}$  as they both exhibit a pronounced linear part, while this feature is missing for  $\Delta\text{VOD}_{\geq 0}$ . The linear part for the original VOD, however, corresponds to the GPP increase, while for  $\Delta\text{VOD}$  the linear part relates to the GPP decrease.

## 4. Discussion

### 4.1. Temporal agreement between VOD, GPP and SIF

In this study, large parts of the world reveal positive correlations

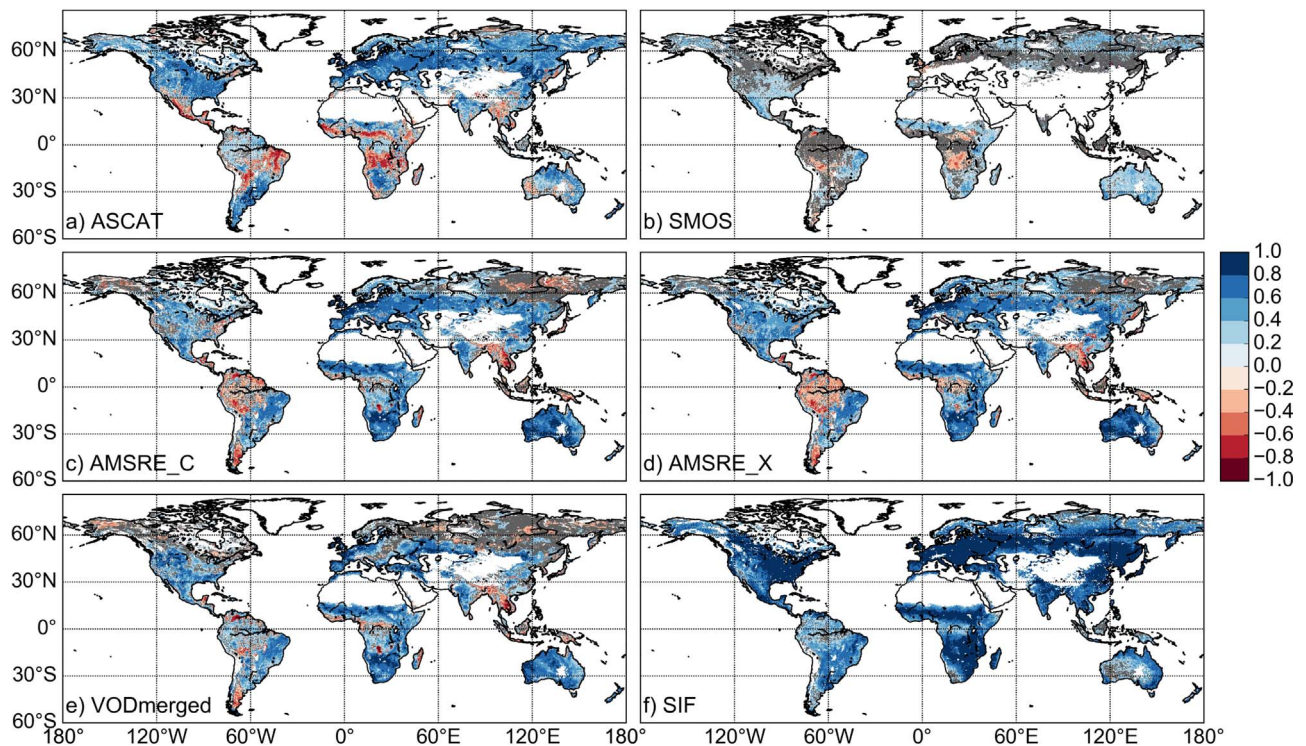


Fig. 2. (a–e) Spearman rank correlation between GPP and VOD data sets at 0.25° and 8-daily resolution. Correlations that are not significant ( $p > 0.05$ ) are masked in grey. Corresponding correlations at 0.5° and monthly resolution are displayed in Fig. S4. (f) Spearman rank correlation between GPP and SIF at 0.5° and monthly resolution.

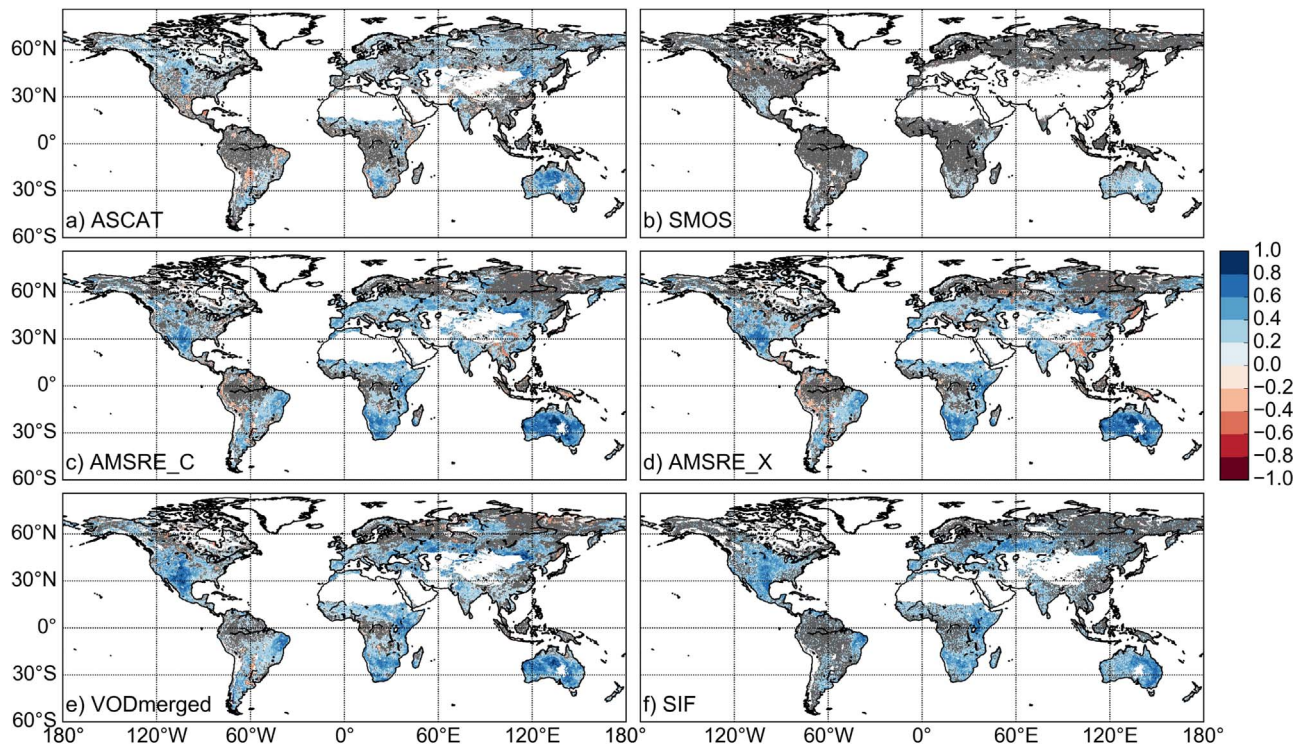
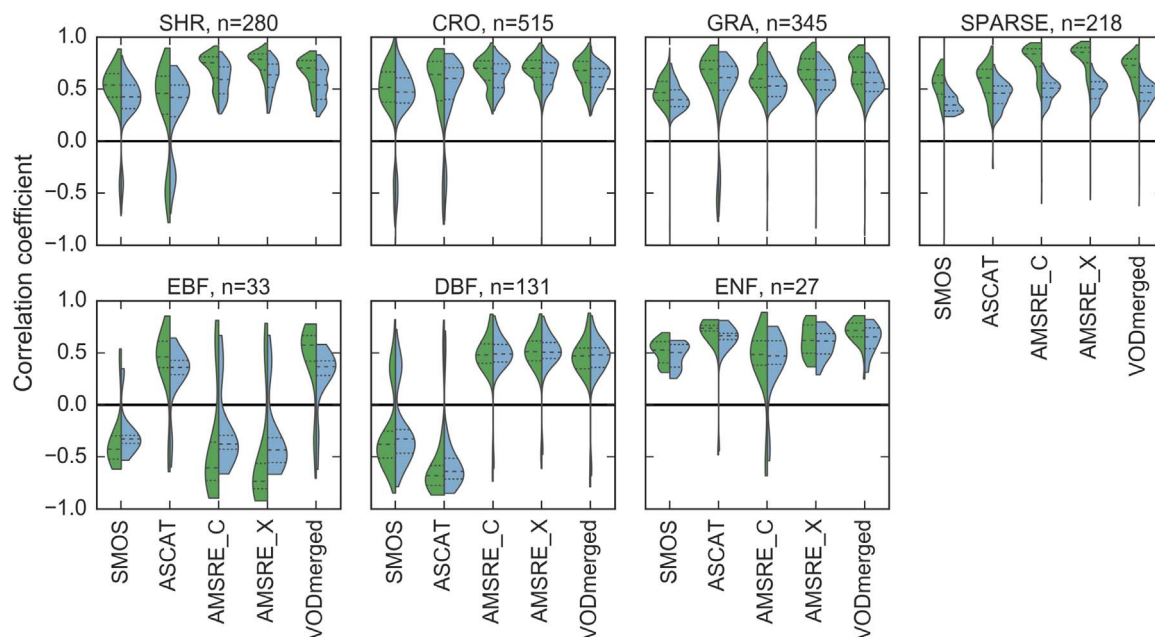


Fig. 3. As Fig. 2 but for the anomalies from the mean seasonal cycle. For a–e, the corresponding correlations at 0.5° and monthly resolution are shown in Fig. S5.

between VOD and GPP both for the original time series and for the anomalies from the mean seasonal cycle. In addition, correlations between VOD and the residuals of the linear GPP-SIF relationship demonstrate that VOD can explain variations in GPP that are not explained by SIF. These findings suggest that VOD provides useful information with regard to GPP.

Water limitation appears to foster the coupling between VOD and GPP as areas with particularly high correlations between VOD and GPP in this study seem to coincide with areas of low water availability (Miralles et al., 2016; Papagiannopoulou et al., 2017). In these areas, vegetation responds more rapidly to changes in water availability (De Keersmaecker et al., 2015), which in turn is reflected in a close



**Fig. 4.** Violin plots of Spearman rank correlation between VOD and GPP (green) and between VOD and SIF (blue) at 0.5° and monthly resolution for grid cells with a dominant land cover fraction above 75%. Results are grouped according to the CCI land cover classification and single frequency data sets are ordered along increasing microwave frequency. The number of grid cells ( $n$ ) is displayed above each graph. Horizontal lines within the violins indicate quartiles. Values that are not significant ( $p > 0.05$ ) are excluded. For the description of the land cover abbreviations see Table 2, for the spatial distribution of grid cells see Fig. 1h. Note that DNF is not displayed since the analysis did not result in significant correlations for this land cover type. (For interpretation of the references to color in this figure legend, the reader is referred to the web version of the article.)

association between VOD and GPP.

The most prominent example of low correlations in this study is found for evergreen broadleaf forests, which can be attributed to the low signal variability found in the tropics. This is in line with the generally low predictability of GPP in tropical forests (Tramontana et al., 2016) and can be linked to isohydricity, which describes the plant strategy of stomatal control in response to water stress (Konings and Gentine, 2016). Evergreen broadleaf forests are very isohydric, i.e. they

try to minimize changes in leaf water potential by closing stomata (Fisher et al., 2006; Konings and Gentine, 2016). This closing of stomata may result in a decoupling of VWC and photosynthetic activity and hence cause a weaker relationship between VOD and GPP.

#### 4.2. Occurrence of negative correlations between VOD and GPP

Negative correlations between VOD and GPP can be attributed to

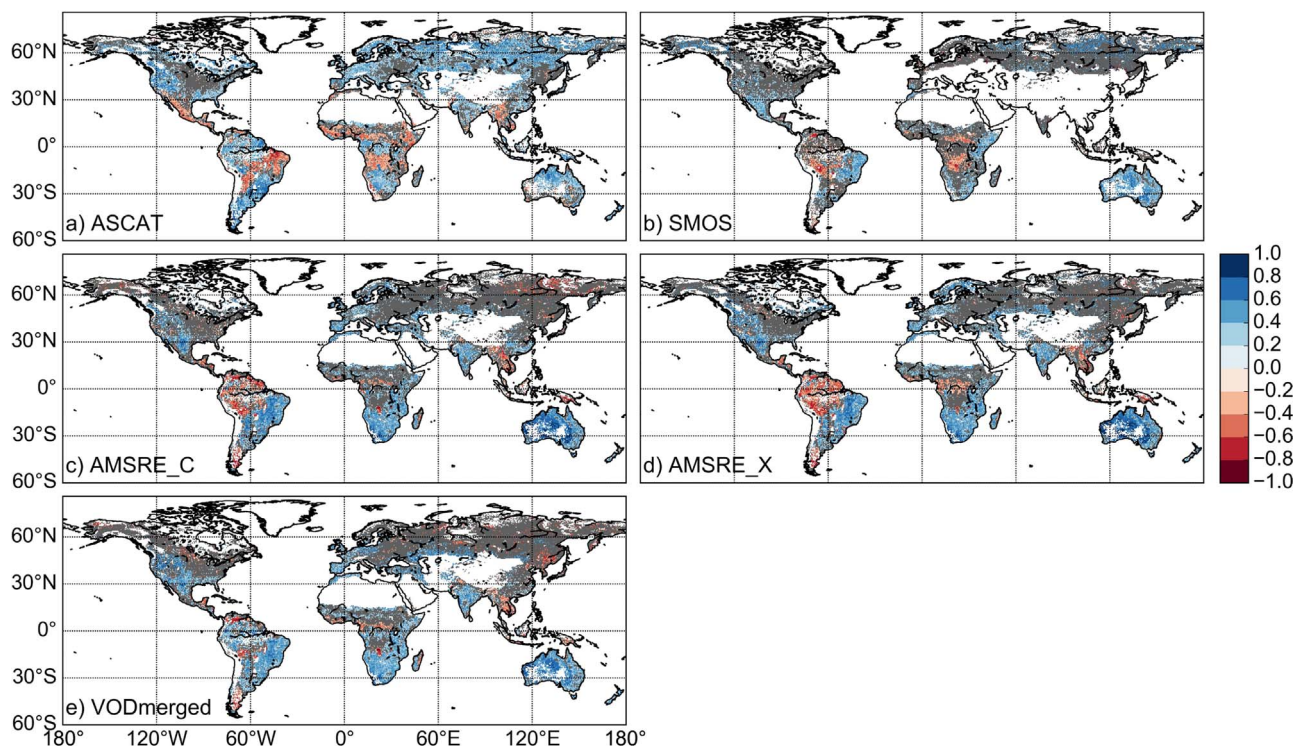


**Fig. 5.** As Fig. 2a–e but for the correlation between VOD and the residuals of the GPP-SIF relationship at 0.5° and monthly resolution.

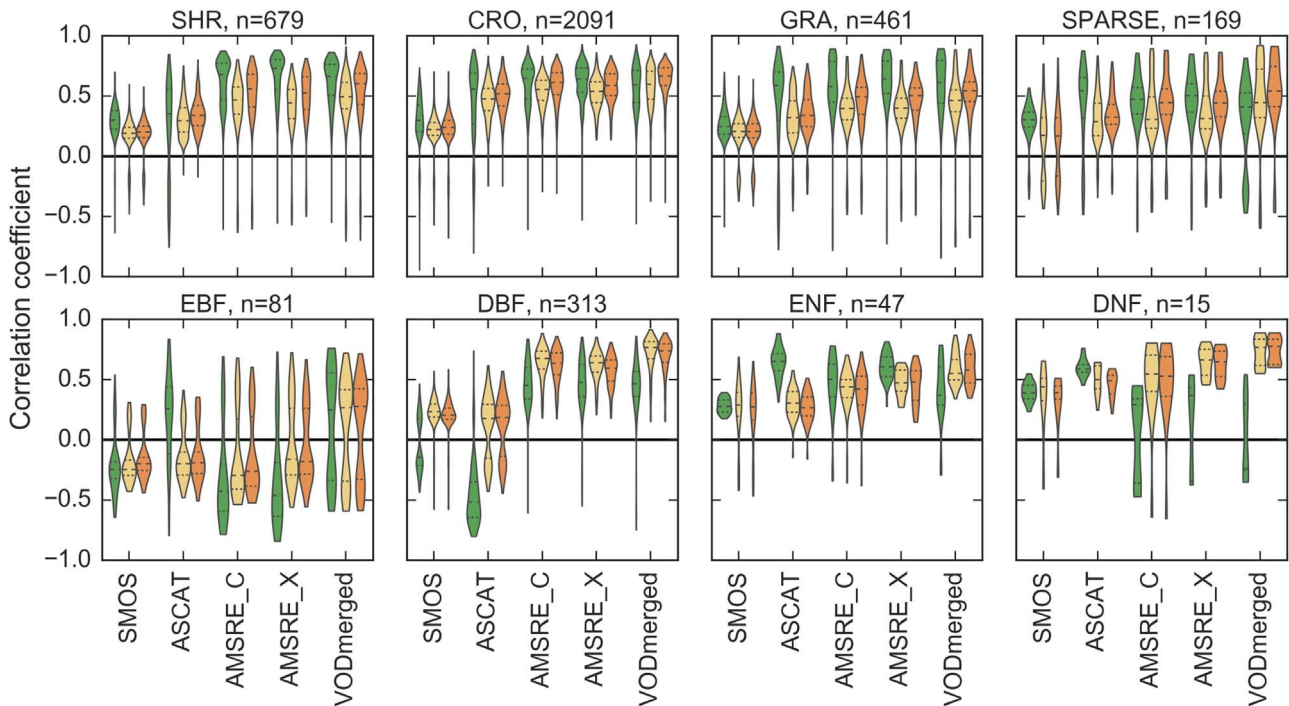


Fig. 6. Violin plots of Spearman rank correlation between GPP and VOD (green),  $\Delta VOD$  (yellow) or  $\Delta VOD_{=0}$  (orange) at 0.25° and 8-daily resolution. Results are displayed for grid cells with a dominant land cover fraction above 75% and grouped according to land cover (Table 2).  $n$  is the number of grid cells. Horizontal lines within the violins indicate quartiles. Values that are not significant ( $p > 0.05$ ) are excluded. See Fig. S3 for the spatial map of the analyzed grid cells. (For interpretation of the references to color in this figure legend, the reader is referred to the web version of the article.)

land surface properties and vegetation phenology. For ASCAT, negative correlations can be explained with the contribution of dry soil to volume scattering (Vreugdenhil et al., 2016a), which is often found for ASCAT backscatter in arid and semi-arid regions (Wagner et al., 2013b; De Jeu et al., 2008). Liu et al. (2016) showed for L-band backscatter that the scattering mechanism of the soil shifts from surface scattering under wet conditions to volume scattering under very dry conditions;

below a certain soil moisture threshold, the backscatter increases again with decreasing soil moisture. Some grid cells showing negative correlations are found in the tropical dry forest biome, which regularly experience a pronounced dry season lasting up to six months (Olivares and Medina, 1992). Therefore, depending on the duration and severity of the seasonal dry period and on the soil properties, volume scattering of dry soil might lead to spurious signals in the VOD if soil volume

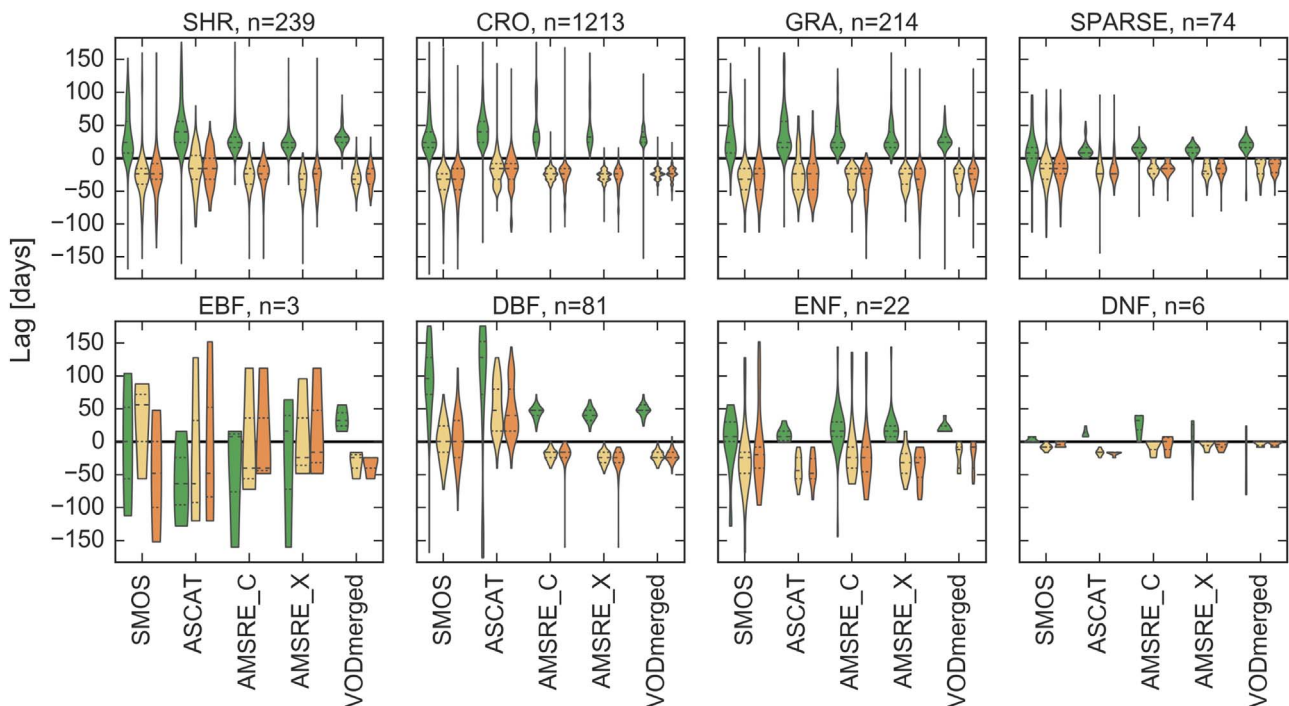
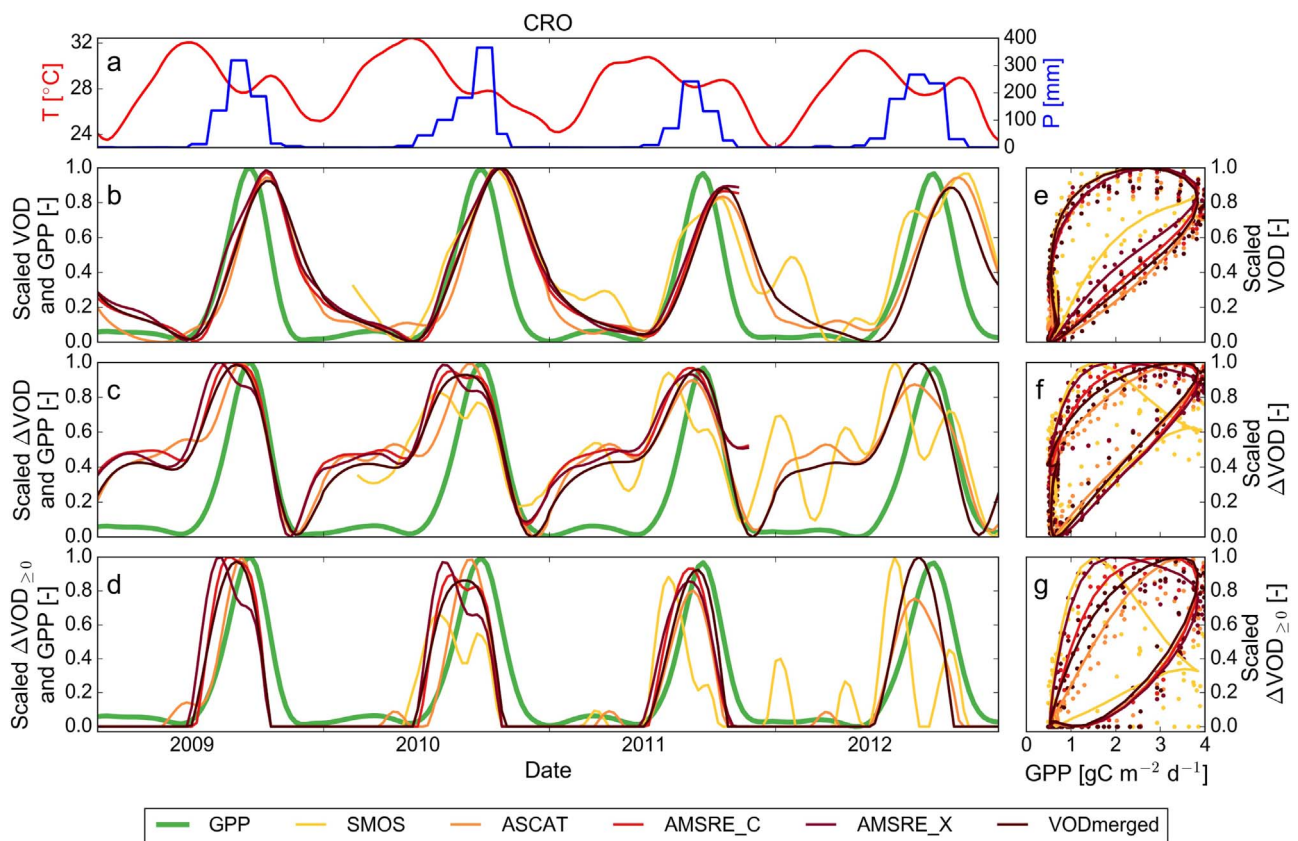


Fig. 7. As Fig. 6 but for the lag. Lag values are excluded if the lag is larger than half a year or the correlation of the lagged time series is not significant ( $p > 0.05$ ).



**Fig. 8.** Time series (a–d) and scatter plots (e–g) at 8-daily resolution for a cropland-dominated grid cell in West Sahel, located at 16.125 W 14.625 N, for the period 2009–2012 (location is indicated in Fig. 1f). (a) Skin temperature ( $T$ ) and monthly sums of precipitation ( $P$ ). (b–d) VOD (b),  $\Delta$ VOD (c), or  $\Delta$ VOD $_{\geq 0}$  (d) together with GPP. Data are smoothed and scaled between their minimum and maximum for visualization purposes. Note that the unscaled  $\Delta$ VOD includes negative values. (e–g) Scatter plots of scaled VOD variables against unscaled GPP for the same data as in (b–d).

scattering is not taken into account in the retrieval algorithm, as is the case for the ASCAT TU-Wien algorithm (Hahn et al., 2017).

In contrast to the active VOD, most negative correlations for passive VOD data can be linked to wetlands (Jones et al., 2011; Liu et al., 2011; Vreugdenhil et al., 2016b). Jones et al. (2011) demonstrated that passive VOD data exhibit an inverse relationship with vegetation growth for areas that are seasonally inundated.

For evergreen broadleaf forest, negative correlations with GPP for SMOS, AMSRE\_C, and AMSRE\_X may partly relate to leaf phenology. Jones et al. (2014) reported asynchronous behavior between flux tower GPP estimates and AMSR-E C-band VOD for the Amazon forest, which may be linked to an inverse relationship between leaf age and photosynthetic capacity. New leaves, which flush during the dry season (Wright and van Schaik, 1994; Huete et al., 2006), are photosynthetically more active than old leaves (Kitajima et al., 2002; Hutyrta et al., 2007) but may also cause overall lower values of VOD.

Similarly, negative correlations found for SMOS in Africa may relate to the phenology in tropical dry forests. Early studies demonstrated that deciduous trees in dry forests minimize their water loss by leaf shedding, and that some trees also flower during the dry season or often leaf out at the end of the dry season (Olivares and Medina, 1992; Borchert, 1994a,b). In terms of the VOD signal, this means that trunks and branches still contain a relatively high amount of water during the dry season. Since L-band data is most sensitive to larger structures (Woodhouse, 2005), this asynchronous behavior of the stem water content may lead to the observed negative correlations between SMOS and GPP.

#### 4.3. Effect of sensor frequency

The comparison of different sensor frequencies between 1 and 10 GHz (L-, C-, and X-band) showed that for sparsely to moderately vegetated areas median correlations increased with sensor frequency. In line with this result, Calvet et al. (2011) demonstrated for a dense wheat field that C- and X-band microwave observations obtained from a ground-based radiometer are more sensitive to VWC than L-band data. Since VWC is linearly related to VOD (Jackson and Schmugge, 1991; Woodhouse, 2005), this can explain the lower magnitude of the correlation coefficients between SMOS and GPP compared to the remaining VOD data sets. For forested regions, a similar behavior, with a low magnitude of the correlation for SMOS, was observed in this study. This suggests that C- and X-band microwave observations are better suited for relating VOD to GPP than L-band data.

#### 4.4. Comparison of the three VOD variables in relation to GPP

Detailed knowledge about land cover is of decisive importance when assessing VOD in relation to GPP. Large differences exist for the three VOD variables between forested and non-forested regions. While  $\Delta$ VOD shows a higher temporal agreement with GPP over forests, the original VOD time series yield higher correlations with GPP for sparsely to moderately vegetated areas.

According to the lag analysis, all three VOD variables generally did not yield a zero lag. The opposite signs for VOD compared to  $\Delta$ VOD and  $\Delta$ VOD $_{\geq 0}$  suggest that at the global scale neither the original VOD time series nor the changes in VOD alone can be used for relating VOD to GPP, but instead should be combined. The reason why both VOD and  $\Delta$ VOD (or  $\Delta$ VOD $_{\geq 0}$ ) are linked to GPP, i.e. the sum of NPP and

autotrophic respiration, can be explained with the contribution of both biomass and growth-related terms to GPP.

NPP relates to the sum of above- and belowground NPP as well as losses through volatile organic compounds (VOC), herbivory and root exudates (Clark et al., 2001a,b; Gower et al., 2001; Girardin et al., 2010). Assuming that belowground NPP is a fraction of ANPP (Clark et al., 2001a), these two terms relate to changes in biomass and, hence, to  $\Delta$ VOD. The magnitude of the VOC flux was estimated to be small compared to NPP or GPP (Guenther et al., 1995; Kesselmeier et al., 2002), and losses through herbivory between consecutive observations and root exudates are difficult to quantify.

Autotrophic respiration can be expressed as the sum of maintenance and growth respiration; while maintenance respiration is proportional to living biomass, growth respiration is a function of the change in biomass (Ryan, 1990; Lavigne et al., 1996). Hence, VOD and  $\Delta$ VOD can be related to maintenance and growth respiration, respectively. This suggests that GPP may be expressed as a combination of VOD and  $\Delta$ VOD.

The relationship between VOD,  $\Delta$ VOD or  $\Delta$ VOD $_{\geq 0}$  and GPP may also vary throughout the season leading to hysteresis as shown in this study for a cropland-dominated grid cell. Similarly, but for the relationship between LAI and GPP, Gitelson et al. (2014) emphasized the importance of seasonal hysteresis. In the current study, the hysteresis was also present for  $\Delta$ VOD, which indicates that this behavior is not merely a result of using a state (VOD) rather than a flux variable ( $\Delta$ VOD). The presence of a seasonal hysteresis also explains here the on average lower correlations found for GPP vs VOD compared to GPP vs SIF, since such a hysteresis decreases the strength of the linear relationship. Combining the original VOD time series and the change in VOD thus might reduce the strength of the seasonal hysteresis and thereby improve the temporal agreement with GPP.

## 5. Conclusion

The global analysis of VOD from different frequencies (L-, C- and X-band) in relation to GPP indicates that microwave VOD, which provides complementary information to optical data, has the potential to serve as explanatory variable for estimating GPP. Although some negative correlations occurred in dry and wet areas for active and passive VOD, respectively, VOD and changes in VOD ( $\Delta$ VOD or  $\Delta$ VOD $_{\geq 0}$ ) generally demonstrated a high temporal agreement with GPP, especially for C- and X-band data. The mainly non-overlapping distributions of negative correlations for active and passive observations indicate that active and passive VOD data should be used jointly. Land cover based differences in lag and correlation coefficient further suggest to combine original VOD time series with changes in VOD for relating VOD to GPP. In addition, seasonal hysteresis was observed for the relationship between VOD variables and GPP, which demonstrates that this relationship may vary both in space and in time. This underpins the need to further investigate the spatio-temporal relationship between VOD and GPP in order to make full use of microwave satellite vegetation data for regional to global ecosystem analyses and vegetation monitoring.

## Acknowledgements

The study is performed as part of the EOWAVE project funded by the TU Wien Wissenschaftspreis 2015 awarded to Wouter Dorigo by the Vienna University of Technology (<http://climbers.geo.tuwien.ac.at/>) with contributions of the STR3S project funded by the Belgian Science Policy Office (BELSPO) as part of the STEREO III program. D G Miralles acknowledges support from the European Research Council (ERC) under grant agreement n° 715254 (DRY-2-DRY).

## Appendix A. Supplementary data

Supplementary data associated with this article can be found, in the

online version, at <http://dx.doi.org/10.1016/j.jag.2017.10.006>.

## References

- Andela, N., Liu, Y.Y., van Dijk, A.I.J.M., de Jeu, R.A.M., McVicar, T.R., Andela, N., Liu, Y.Y., van Dijk, A.I.J.M., de Jeu, R.A.M., McVicar, T.R., 2013. Global changes in dryland vegetation dynamics (1988–2008) assessed by satellite remote sensing: comparing a new passive microwave vegetation density record with reflective greenness data. *Biogeosciences* 10 (10), 6657–6676 <http://www.biogeosciences.net/10/6657/2013>.
- Baldocchi, D., Falge, E., Gu, L., Olson, R., Hollinger, D., Running, S., Anthoni, P., Bernhofer, C., Davis, K., Evans, R., Fuentes, J., Goldstein, A., Katul, G., Law, B., Lee, X., Malhi, Y., Meyers, T., Munger, W., Oechel, W., Paw, K.T., Pilegaard, K., Schmid, H.P., Valentini, R., Verma, S., Vesala, T., Wilson, K., Wofsy, S., 2001. FLUXNET: a new tool to study the temporal and spatial variability of ecosystem-scale carbon dioxide, water vapor, and energy flux densities. *Bull. Am. Meteorol. Soc.* 82 (11), 2415–2434. [http://dx.doi.org/10.1175/1520-0477\(2001\)082<3C2415:FAFANTTS3E2.3.CO;2](http://dx.doi.org/10.1175/1520-0477(2001)082<3C2415:FAFANTTS3E2.3.CO;2).
- Beer, C., Reichstein, M., Tomelleri, E., Ciais, P., Jung, M., Carvalhais, N., Röenbeck, C., Arain, M.A., Baldocchi, D., Bonan, G.B., Bondeau, A., Cescatti, A., Lasslop, G., Lindroth, A., Lomas, M., Luysaert, S., Margolis, H., Oleson, K.W., Rouspard, O., Veenendaal, E., Viovy, N., Williams, C., Woodward, F.I., Papale, D., 2010. Terrestrial gross carbon dioxide uptake: global distribution and covariation with climate. *Science* 329 (5993), 834–838. <http://science.sciencemag.org/content/329/5993/834>.
- Bonan, G., 2015. *Ecological Climatology: Concepts and Applications*. [https://books.google.at/books/about/Ecological\\_Climatology.html?id=kq8kDQAAQBAJ](https://books.google.at/books/about/Ecological_Climatology.html?id=kq8kDQAAQBAJ).
- Bonan, G.B., 2008. Forests and climate change: forcings, feedbacks, and the climate benefits of forests. *Science* 320 (5882), 1444–1449. <http://science.sciencemag.org/content/320/5882/1444>.
- Bontemps, S., Defourny, P., Radoux, J., Van Bogaert, E., Lamarche, C., Achard, F., Mayaux, P., Boettcher, M., Brockmann, C., Kirches, G., Zülke, M., Kalogirou, V., Seifert, F.M., Arino, O., 2013. Consistent global land cover maps for climate modelling communities: current achievements of the ESA' Land cover CCI. In: *ESA Living Planet Symposium 2013*. Edinburgh, UK. [https://ftp.space.dtu.dk/pub/loana/papers/s274\\_2bont.pdf](https://ftp.space.dtu.dk/pub/loana/papers/s274_2bont.pdf).
- Borchert, R., 1994a. Soil and stem water storage determine phenology and distribution of tropical dry forest trees. *Ecology* 75 (5), 1437–1449. <http://dx.doi.org/10.2307/1937467/abstract>.
- Borchert, R., 1994b. Water status and development of tropical trees during seasonal drought. *Trees* 8 (3), 115–125. <http://dx.doi.org/10.1007/BF00196635>.
- Calvet, J.-C., Wigneron, J.-P., Walker, J., Karbou, F., Chanzy, A., Albergel, C., 2011. Sensitivity of passive microwave observations to soil moisture and vegetation water content: L-band to W-band. *IEEE Trans. Geosci. Remote Sens.* 49 (9), 1190–1199. <https://www.infona.pl/resource/bwmeta1.element.ieee-art-000005492186>.
- Campioi, M., Gielen, B., Gökcede, M., Papale, D., Bouriaud, O., Granier, A., 2011. Temporal variability of the NPP-GPP ratio at seasonal and interannual time scales in a temperate beech forest. *Biogeosciences* 8 (9), 2481–2492 <http://www.biogeosciences.net/8/2481/2011/>.
- Campioi, M., Malhi, Y., Vicca, S., Luysaert, S., Papale, D., Peñuelas, J., Reichstein, M., Migliavacca, M., Arain, M.A., Janssens, I.A., 2016. Evaluating the convergence between eddy-covariance and biometric methods for assessing carbon budgets of forests. *Nat. Commun.* 7, 13717. <http://www.nature.com/ncomms/2016/161214/ncomms13717/full/ncomms13717.html>.
- Chen, J., Jönsson, P., Tamura, M., Gu, Z., Matsushita, B., Eklundh, L., 2004. A simple method for reconstructing a high-quality NDVI time-series data set based on the Savitzky-Golay filter. *Remote Sens. Environ.* 91 (3–4), 332–344. <http://www.sciencedirect.com/science/article/pii/S003442570400080X>.
- Ciais, P., Sabine, C., Bala, G., Bopp, L., Brovkin, V., Canadell, J., Chhabra, A., DeFries, R., Galloway, J., Heimann, M., Jones, C., Le Quéré, C., Myneni, R.B., Piao, S., Thornton, P., 2013. Carbon and other biogeochemical cycles. In: *Stocker, T., Qin, D., Plattner, G.-K., Tignor, M., Allen, S., Boschung, J., Nauels, A., Xia, Y., Bex, V., Midgley, P. (Eds.), Climate Change 2013: The Physical Science Basis*. Contribution of Working Group I to the Fifth Assessment Report of the Intergovernmental Panel on Climate Change. Cambridge University Press, Cambridge, United Kingdom/New York, NY, USA.
- Clark, D.A., Brown, S., Kicklighter, D.W., Chambers, J.Q., Thomlinson, J.R., Ni, J., 2001a. Measuring net primary production in forests: concepts and field methods. *Ecol. Appl.* 11 (2), 356–370. [http://dx.doi.org/10.1890/1051-0761\(2001\)011\[0356:MNPPIF\]2.0.CO;2/abstract](http://dx.doi.org/10.1890/1051-0761(2001)011[0356:MNPPIF]2.0.CO;2/abstract).
- Clark, D.A., Brown, S., Kicklighter, D.W., Chambers, J.Q., Thomlinson, J.R., Ni, J., Holland, E.A., 2001b. Net primary production in tropical forests: an evaluation and synthesis of existing field data. *Ecol. Appl.* 11 (2), 371–384 [ftp://ftp.orest.sr.unh.edu/pub/MLSmith/John\\_20R/Backup/NPP\\_carbon\\_20pub/i1051-0761-011-02-0371.pdf](ftp://ftp.orest.sr.unh.edu/pub/MLSmith/John_20R/Backup/NPP_carbon_20pub/i1051-0761-011-02-0371.pdf).
- Collatz, G.J., Ribas-Carbo, M., Berry, J.A., Collatz, G.J., Ribas-Carbo, M., Berry, J.A., 1992. Coupled photosynthesis-stomatal conductance model for leaves of C4 plants. *Funct. Plant Biol.* 19 (5), 519–538. <http://www.publish.csiro.au/fp/PP9920519>.
- D'Agostino, R., Pearson, E.S., 1973. Tests for departure from normality. Empirical results for the distributions of  $b_2$  and  $\sqrt{b_1}$ . *Biometrika* 60 (3), 613–622. <http://biomet.oxfordjournals.org/content/60/3/613>.
- D'Agostino, R.B., 1971. An omnibus test of normality for moderate and large size samples. *Biometrika* 58 (2), 341–348. <http://biomet.oxfordjournals.org/content/58/2/341>.
- Damm, A., Guanter, L., Paul-Limoges, E., van der Tol, C., Hueni, A., Buchmann, N., Eugster, W., Ammann, C., Schaepman, M.E., 2015. Far-red sun-induced chlorophyll

- fluorescence shows ecosystem-specific relationships to gross primary production: an assessment based on observational and modeling approaches. *Remote Sens. Environ.* 166, 91–105. <http://www.sciencedirect.com/science/article/pii/S0034425715300341>.
- De Jeu, R.A.M., Wagner, W., Holmes, T.R.H., Dolman, A.J., Giesen, N.C.v.d., Friesen, J., 2008. Global soil moisture patterns observed by space borne microwave radiometers and scatterometers. *Surv. Geophys.* 29 (4–5), 399–420. <http://dx.doi.org/10.1007/s10712-008-9044-0>.
- De Keersmaecker, W., Lhermitte, S., Tits, L., Honnay, O., Somers, B., Coppin, P., 2015. A model quantifying global vegetation resistance and resilience to short-term climate anomalies and their relationship with vegetation cover: global vegetation resistance and resilience. *Glob. Ecol. Biogeogr.* 24 (5), 539–548. <http://dx.doi.org/10.1111/geb.12279>.
- Dee, D.P., Uppala, S.M., Simmons, A.J., Berrisford, P., Poli, P., Kobayashi, S., Andrae, U., Balmaseda, M.A., Balsamo, G., Bauer, P., Bechtold, P., Beljaars, A.C.M., van de Berg, L., Bidlot, J., Bormann, N., Delsol, C., Dragani, R., Fuentes, M., Geer, A.J., Haimberger, L., Healy, S.B., Hersbach, H., Hölm, E.V., Isaksen, I., Källberg, P., Köhler, M., Matricardi, M., McNally, A.P., Monge-Sanz, B.M., Morcrette, J.-J., Park, B.-K., Peubey, C., de Rosnay, P., Tavolato, C., Thépaut, J.-N., Vitart, F., 2011. The ERA-interim reanalysis: configuration and performance of the data assimilation system. *Q. J. R. Meteorol. Soc.* 137 (656), 553–597. <http://dx.doi.org/10.1002/qj.828/abstract>.
- Dorigo, W.A., 2012. Improving the robustness of cotton status characterisation by radiative transfer model inversion of multi-angular CHRIS/PROBA data. *IEEE J. Select. Top. Appl. Earth Observ. Remote Sens.* 5 (1), 18–29.
- Dorigo, W.A., Gruber, A., De Jeu, R.A.M., Wagner, W., Stacke, T., Loew, A., Albergel, C., Brocca, L., Chung, D., Parinussa, R.M., Kidd, R., 2015. Evaluation of the ESA CCI soil moisture product using ground-based observations. *Remote Sens. Environ.* 162, 380–395. <http://www.sciencedirect.com/science/article/pii/S0034425714002727>.
- Dorigo, W.A., Zurita-Milla, R., de Wit, A.J.W., Brazile, J., Singh, R., Schaepman, M.E., 2007. A review on reflective remote sensing and data assimilation techniques for enhanced agroecosystem modeling. *Int. J. Appl. Earth Observ. Geoinf.* 9 (2), 165–193. <http://www.sciencedirect.com/science/article/pii/S0303243406000201>.
- Draper, C.S., Reichle, R.H., Lannoy, D.M.G.J., Liu, Q., 2012. Assimilation of passive and active microwave soil moisture retrievals. *Geophys. Res. Lett.* 39 (4). <http://dx.doi.org/10.1029/2011GL050655/abstract>.
- Farquhar, G.D., Caemmerer, S.V., Berry, J.A., 1980. A biochemical model of photosynthetic CO<sub>2</sub> assimilation in leaves of C<sub>3</sub> species. *Planta* 149 (1), 78–90. <http://dx.doi.org/10.1007/BF00386231>.
- Fisher, R.A., Williams, M., Vale, D., Lobo, R., Costa, D., Lola, A., Meir, P., 2006. Evidence from amazonian forests is consistent with isohydric control of leaf water potential. *Plant Cell Environ.* 29 (2), 151–165. <http://dx.doi.org/10.1111/j.1365-3040.2005.01407.x/full>.
- Forkel, M., Carvalhais, N., Verbesselt, J., Mahecha, M.D., Neigh, C.S.R., Reichstein, M., 2013. Trend change detection in NDVI time series: effects of inter-annual variability and methodology. *Remote Sens.* 5 (5), 2113–2144. <http://www.mdpi.com/2072-4292/5/5/2113>.
- Frankenberg, C., O'Dell, C., Berry, J., Guanter, L., Joiner, J., Köhler, P., Pollock, R., Taylor, T.E., 2014. Prospects for chlorophyll fluorescence remote sensing from the orbiting carbon observatory-2. *Remote Sens. Environ.* 147, 1–12. <http://linkinghub.elsevier.com/retrieve/pii/S0034425714000522>.
- Girardin, C.A.J., Malhi, Y., Aragão, L.E.O.C., Mamani, M., Huaraca Huasco, W., Durand, L., Feeley, K.J., Rapp, J., Silva-Espejo, J.E., Silman, M., Salinas, N., Whittaker, R.J., 2010. Net primary productivity allocation and cycling of carbon along a tropical forest elevational transect in the Peruvian Andes. *Glob. Change Biol.* 16 (12), 3176–3192. <http://dx.doi.org/10.1111/j.1365-2486.2010.02235.x/full>.
- Gitelson, A.A., Peng, Y., Arkebauer, T.J., Schepers, J., 2014. Relationships between gross primary production, green LAI, and canopy chlorophyll content in maize: Implications for remote sensing of primary production. *Remote Sens. Environ.* 144, 65–72. <http://www.sciencedirect.com/science/article/pii/S0034425714000170>.
- Gower, S.T., Krankina, O., Olson, R.J., Apps, M., Linder, S., Wang, C., 2001. Net primary production and carbon allocation patterns of boreal forest ecosystems. *Ecol. Appl.* 11 (5), 1395–1411. [http://dx.doi.org/10.1890/1051-0761\(2001\)011\[1395:NPPACA\]2.0.CO;2/full](http://dx.doi.org/10.1890/1051-0761(2001)011[1395:NPPACA]2.0.CO;2/full).
- Guanter, L., Zhang, Y., Jung, M., Joiner, J., Voigt, M., Berry, J.A., Frankenberg, C., Huete, A.R., Zarco-Tejada, P., Lee, J.-E., Moran, M.S., Ponce-Campos, G., Beer, C., Camps-Valls, G., Buchmann, N., Gianelle, D., Klumpp, K., Cescatti, A., Baker, J.M., Griffis, T.J., 2014. Global and time-resolved monitoring of crop photosynthesis with chlorophyll fluorescence. *Proc. Natl. Acad. Sci. U. S. A.* 111 (14), E1327–E1333. <http://www.pnas.org/content/111/14/E1327>.
- Guenther, A., Hewitt, C.N., Erickson, D., Fall, R., Geron, C., Graedel, T., Harley, P., Klinger, L., Lerdau, M., McKay, W.A., Pierce, T., Scholes, B., Steinbrecher, R., Tallamraju, R., Taylor, J., Zimmerman, P., 1995. A global model of natural volatile organic compound emissions. *J. Geophys. Res.* 100 (D5), 8873–8892. <http://dx.doi.org/10.1029/94JD02950>.
- Hahn, S., Reimer, C., Vreugdenhil, M., Melzer, T., Wagner, W., 2017. Dynamic characterization of the incidence angle dependence of backscatter using metop ASCAT. *IEEE J. Select. Top. Appl. Earth Observ. Remote Sens.* PP (99), 1–12.
- Holben, B.N., 1986. Characteristics of maximum-value composite images from temporal AVHRR data. *Int. J. Remote Sens.* 7 (11), 1417–1434. <http://dx.doi.org/10.1080/01431168608948945>.
- Huete, A., Didan, K., Leeuwen, W.v., Miura, T., Glenn, E., 2011. MODIS vegetation indices. *Land Remote Sens. Glob. Environ. Change* 579–602. [http://dx.doi.org/10.1007/978-1-4419-6749-7\\_26](http://dx.doi.org/10.1007/978-1-4419-6749-7_26).
- Huete, A.R., Didan, K., Shimabukuro, Y.E., Ratana, P., Saleska, S.R., Hutrya, L.R., Yang, W., Nemani, R.R., Myneni, R., 2006. Amazon rainforests green-up with sunlight in dry season. *Hydrol. Land Surf. Stud.* 33 (6). <http://dx.doi.org/10.1029/2005GL025583/full>.
- Huffman, G.J., Adler, R.F., Morrissey, M.M., Bolvin, D.T., Curtis, S., Joyce, R., McGavock, B., Susskind, J., 2001. Global precipitation at one-degree daily resolution from multisatellite observations. *J. Hydrometeorol.* 2 (1), 36–50. [http://dx.doi.org/10.1175/1525-7541\(2001\)0023C00363AGPAODD3E2.0.CO;3B2](http://dx.doi.org/10.1175/1525-7541(2001)0023C00363AGPAODD3E2.0.CO;3B2).
- Hutrya, L.R., Munger, J.W., Saleska, S.R., Gottlieb, E., Daube, B.C., Dunn, A.L., Amaral, D.F., Camargo, D.B.P., Wofsy, S.C., 2007. Seasonal controls on the exchange of carbon and water in an amazonian rain forest. *J. Geophys. Res.* 112. <http://dx.doi.org/10.1029/2006JG000365/full>.
- Jackson, T.J., Schmugge, T.J., 1991. Vegetation effects on the microwave emission of soils. *Remote Sens. Environ.* 36 (3), 203–212. <http://www.sciencedirect.com/science/article/pii/003442579190057D>.
- Joiner, J., Guanter, L., Lindström, R., Voigt, M., Vasilkov, A.P., Middleton, E.M., Huemmrich, K.F., Yoshida, Y., Frankenberg, C., 2013. Global monitoring of terrestrial chlorophyll fluorescence from moderate-spectral-resolution near-infrared satellite measurements: methodology, simulations, and application to GOME-2. *Atmos. Meas. Tech.* 6, 2803–2823. <http://www.atmos-meas-tech.net/6/2803/2013/amt-6-2803-2013.pdf>.
- Joiner, J., Yoshida, Y., Guanter, L., Middleton, E.M., 2016. New methods for the retrieval of chlorophyll red fluorescence from hyperspectral satellite instruments: simulations and application to GOME-2 and SCIAMACHY. *Atmos. Meas. Tech.* 9 (8), 3939–3967. <http://www.atmos-meas-tech.net/9/3939/2016/amt-9-3939-2016-discussion.html>.
- Joiner, J., Yoshida, Y., Vasilkov, A.P., Schaefer, K., Jung, M., Guanter, L., Zhang, Y., Garrity, S., Middleton, E.M., Huemmrich, K.F., Gu, L., Belleli Marchesini, L., 2014. The seasonal cycle of satellite chlorophyll fluorescence observations and its relationship to vegetation phenology and ecosystem atmosphere carbon exchange. *Remote Sens. Environ.* 152, 375–391. <http://www.sciencedirect.com/science/article/pii/S0034425714002429>.
- Jones, M.O., Jones, L.A., Kimball, J.S., McDonald, K.C., 2011. Satellite passive microwave remote sensing for monitoring global land surface phenology. *Remote Sens. Environ.* 115 (4), 1102–1114. <http://www.sciencedirect.com/science/article/pii/S0034425710003615>.
- Jones, M.O., Kimball, J.S., Jones, L.A., McDonald, K.C., 2012. Satellite passive microwave detection of North America start of season. *Remote Sens. Environ.* 123, 324–333. <http://www.sciencedirect.com/science/article/pii/S0034425712001575>.
- Jones, M.O., Kimball, J.S., Nemani, R.R., 2014. Asynchronous Amazon forest canopy phenology indicates adaptation to both water and light availability. *Environ. Res. Lett.* 9 (12), 124021. <http://stacks.iop.org/1748-9326/9/i=12/a=124021?key=crossref.10b2710176d7cd3ad2f6d5d1d5fa1e07>.
- Jung, M., Reichstein, M., Margolis, H.A., Cescatti, A., Richardson, A.D., Arain, M.A., Arnett, A., Bernhofer, C., Bonal, D., Chen, J., Gianelle, D., Gobron, N., Kiely, G., Kutsch, W., Lasslop, G., Law, B.E., Lindroth, A., Merbold, L., Montagnani, L., Moors, E.J., Papale, D., Sottocornola, M., Vaccari, F., Williams, C., 2011. Global patterns of land-atmosphere fluxes of carbon dioxide, latent heat, and sensible heat derived from eddy covariance, satellite, and meteorological observations. *J. Geophys. Res.* 116 (G3), G00J07. <http://dx.doi.org/10.1029/2010JG001566>.
- Kesselmeier, J., Ciccioli, P., Kuhn, U., Stefani, P., Biesenthal, T., Rottenberger, S., Wolf, A., Vitullo, M., Valentini, R., Nobre, A., Kabat, P., Andreae, M.O., 2002. Volatile organic compound emissions in relation to plant carbon fixation and the terrestrial carbon budget. *Glob. Biogeochem. Cycles* 16 (4). <http://dx.doi.org/10.1029/2001GB001813/full>.
- Kim, Y., Jackson, T., Bindlish, R., Lee, H., Hong, S., 2012. Radar vegetation index for estimating the vegetation water content of rice and soybean. *IEEE Geosci. Remote Sens. Lett.* 9 (4), 564–568.
- Kitajima, K., Mulkey, S.S., Samaniego, M., Wright, S.J., 2002. Decline of photosynthetic capacity with leaf age and position in two tropical pioneer tree species. *Am. J. Bot.* 89 (12), 1925–1932. <http://www.amjbot.org/content/89/12/1925>.
- Kokoska, S., Zwillinger, D., 2000. *CRC Standard Probability and Statistics Tables and Formulae*, Student ed. CRC Press, google-Books-ID 5G5hJqwJweUc.
- Konings, A.G., Gentile, P., 2016. Global variations in ecosystem-scale isohydricity. *Glob. Change Biol.* 23 (2), 891–905. <http://dx.doi.org/10.1111/gcb.13389>.
- Lambers, H., Chapin, F.S.L., Pons, T.L., 2008. *Plant Physiological Ecology*. Springer Science & Business Media. [https://books.google.at/books/about/Plant\\_Physiological\\_Ecology.html?hl=de&id=PXBA6qjT5SYC](https://books.google.at/books/about/Plant_Physiological_Ecology.html?hl=de&id=PXBA6qjT5SYC).
- Lasslop, G., Migliavacca, M., Bohrer, G., Reichstein, M., Bahn, M., Ibrom, A., Jacobs, C., Kolari, P., Papale, D., Vesala, T., Wohlfahrt, G., Cescatti, A., 2012. On the choice of the driving temperature for eddy-covariance carbon dioxide flux partitioning. *Biogeosciences* 9 (12), 5243–5259. <http://www.biogeosciences.net/9/5243/2012/>.
- Lavigne, M., Franklin, S., Hunt Jr, E.R., 1996. Estimating stem maintenance respiration rates of dissimilar balsam fir stands. *Tree Physiol.* 16, 687–695. [https://www.researchgate.net/profile/Michael\\_Lavigne2/publication/8778227\\_Estimating\\_stem\\_maintenance\\_respiration\\_rates\\_of\\_dissimilar\\_balsam\\_fir\\_stands/links/02e7e51819154d8e72000000.pdf](https://www.researchgate.net/profile/Michael_Lavigne2/publication/8778227_Estimating_stem_maintenance_respiration_rates_of_dissimilar_balsam_fir_stands/links/02e7e51819154d8e72000000.pdf).
- Li, L., Njoku, E.G., Im, E., Chang, P.S., Germain, K.S., 2004. A preliminary survey of radio-frequency interference over the U.S. in aqua AMSR-e data. *IEEE Trans. Geosci. Remote Sens.* 42 (2), 380–390.
- Liu, P.-W., Judge, J., DeRoo, R.D., England, A.W., Bongiovanni, T., Luke, A., 2016. Dominant backscattering mechanisms at L-band during dynamic soil moisture conditions for sandy soils. *Remote Sens. Environ.* 178, 104–112. <http://www.sciencedirect.com/science/article/pii/S0034425716300918>.
- Liu, Y.Y., Evans, J.P., McCabe, M.F., de Jeu, R.A.M., van Dijk, A.I.J.M., Dolman, A.J., Saizen, I., 2013a. Changing climate and overgrazing are decimating mongolian steppes. *PLoS ONE* 8 (2), e57599. <http://dx.doi.org/10.1371/journal.pone.0057599>.
- Liu, Y.Y., Jeu, R.A.M., McCabe, M.F., Evans, J.P., van Dijk, A.I.J.M., 2011. Global long-term passive microwave satellite-based retrievals of vegetation optical depth. *Geophys.*

- Res. Lett. 38 (18). <http://dx.doi.org/10.1029/2011GL048684/abstract>.
- Liu, Y.Y., van Dijk, A.I.J.M., de Jeu, R.A.M., Canadell, J.G., McCabe, M.F., Evans, J.P., Wang, G., 2015. Recent reversal in loss of global terrestrial biomass. *Nat. Clim. Change* 5 (5), 470–474. <http://dx.doi.org/10.1038/nclimate2581>.
- Liu, Y.Y., van Dijk, A.I.J.M., de Jeu, R.A.M., Holmes, T.R.H., 2009. An analysis of spatiotemporal variations of soil and vegetation moisture from a 29-year satellite-derived data set over mainland Australia. *Water Resour. Res.* 45 (7), W07405. <http://dx.doi.org/10.1029/2008WR007187/abstract>.
- Liu, Y.Y., van Dijk, A.I.J.M., McCabe, M.F., Evans, J.P., de Jeu, R.A.M., 2013b. Global vegetation biomass change (1988–2008) and attribution to environmental and human drivers: Global vegetation biomass change. *Global Ecol. Biogeogr.* 22 (6), 692–705. <http://dx.doi.org/10.1111/geb.12024>.
- Marle, M.v., Werf, G.v.d., Jeu, R.d., Liu, Y., 2016. Annual South American forest loss estimates based on passive microwave remote sensing (1990–2010). *Biogeosciences* 13 (2), 609–624. <http://www.biogeosciences.net/13/609/2016/bg-13-609-2016-relations.html>.
- Martens, B., Miralles, D.G., Lievens, H., van der Schalie, R., de Jeu, R.A.M., Fernández-Prieto, D., Beck, H.E., Dorigo, W.A., Verhoest, N.E.C., 2016. GLEAM v3: satellite-based land evaporation and root-zone soil moisture. *Geoscientific Model Development Discussions*. pp. 1–36. <http://www.geosci-model-dev-discuss.net/gmd-2016-162/>.
- Meesters, A.G.C.A., Jeu, R.A.M.D., Owe, M., 2005. Analytical derivation of the vegetation optical depth from the microwave polarization difference index. *IEEE Geosci. Remote Sens. Lett.* 2 (2), 121–123. <http://ieeexplore.ieee.org/articleDetails.jsp?arnumber=1420287>.
- Melzer, T., 2013. Vegetation modelling in WARP 6.0. In: *Understanding the Past, Observing the Present and Protecting the Future Vienna 2013*. Vienna, Austria.
- Miralles, D.G., Holmes, T.R.H., De Jeu, R.A.M., Gash, J.H., Meesters, A.G.C.A., Dolman, A.J., 2011. Global land-surface evaporation estimated from satellite-based observations. *Hydrol. Earth Syst. Sci.* 15 (2), 453–469. <http://search.proquest.com/openview/e97bc7142dade93942375ef83bde1590/1?pq-origsite=gscholar&cbl=105724>.
- Miralles, D.G., Nieto, R., McDowell, N.G., Dorigo, W.A., Verhoest, N.E., Liu, Y.Y., Teuling, A.J., Dolman, A.J., Good, S.P., Gimeno, L., 2016. Contribution of water-limited ecoregions to their own supply of rainfall. *Environ. Res. Lett.* 11 (12), 124007. <http://dx.doi.org/10.1088/1748-9326/11/12/124007/meta>.
- Mo, T., Choudhury, B.J., Schmugge, T.J., Wang, J.R., Jackson, T.J., 1982. A model for microwave emission from vegetation-covered fields. *J. Geophys. Res.: Oceans* 87 (C13), 11229–11237. <http://dx.doi.org/10.1029/JC087iC13p11229.full>.
- Monteith, J.L., 1972. Solar radiation and productivity in tropical ecosystems. *J. Appl. Ecol.* 9 (3), 747–766. <http://www.jstor.org/stable/2401901>.
- Morton, D.C., Nagol, J., Carabajal, C.C., Rosette, J., Palace, M., Cook, B.D., Vermote, E.F., Harding, D.J., North, P.R.J., 2014. Amazon forests maintain consistent canopy structure and greenness during the dry season. *Nature* 506 (7487), 221–224. <http://dx.doi.org/10.1038/nature13006>.
- Myneni, R.B., Hoffman, S., Knyazikhin, Y., Privette, J.L., Glassy, J., Tian, Y., Wang, Y., Song, X., Zhang, Y., Smith, G.R., Lott, A., Friedl, M., Morisette, J.T., Votava, P., Nemani, R.R., Running, S.W., 2002. Global products of vegetation leaf area and fraction absorbed PAR from year one of MODIS data. *Remote Sens. Environ.* 83 (1–2), 214–231. <http://www.sciencedirect.com/science/article/pii/S0034425702000743>.
- Nemani, R.R., Keeling, C.D., Hashimoto, H., Jolly, W.M., Piper, S.C., Tucker, C.J., Myneni, R.B., Running, S.W., 2003. Climate-driven increases in global terrestrial net primary production from 1982 to 1999. *Science* 300 (5625), 1560–1563. <http://science.sciencemag.org/content/300/5625/1560>.
- Njoku, E.G., Ashcroft, P., Chan, T.K., Li, L., 2005. Global survey and statistics of radio-frequency interference in AMSR-e land observations 43 (5), 938–947.
- Nunes, L., Lopes, D., Castro Rego, F., Gower, S.T., 2013. Aboveground biomass and net primary production of pine, oak and mixed pine-oak forests on the Vila Real district, Portugal. *Forest Ecol. Manag.* 305, 38–47. <https://www.sciencedirect.com/science/article/pii/S0378112713003332>.
- Olivares, E., Medina, E., 1992. Water and nutrient relations of woody perennials from tropical dry forests. *J. Veg. Sci.* 3 (3), 383–392. <http://dx.doi.org/10.2307/3235764/full>.
- Owe, M., de Jeu, R., Holmes, T., 2008. Multisensor historical climatology of satellite-derived global land surface moisture. *J. Geophys. Res.* 113, F01002. <http://dx.doi.org/10.1029/2007JF000769/abstract>.
- Owe, M., Jeu, R.d., Walker, J., 2001. A methodology for surface soil moisture and vegetation optical depth retrieval using the microwave polarization difference index. *IEEE Trans. Geosci. Remote Sens.* 39 (8), 1643–1654. <http://ieeexplore.ieee.org/articleDetails.jsp?arnumber=942542>.
- Papagiannopoulou, C., Miralles, D.G., Dorigo, W.A., Verhoest, N.E.C., Depoorter, M., Waegeman, W., 2017. Vegetation anomalies caused by antecedent precipitation in most of the world. *Environ. Res. Lett.* 12 (7), 074016. <http://stacks.iop.org/1748-9326/12/i=7/a=074016?key=crossref.aec129902b307d6614b07d44903e2fe7>.
- Reichstein, M., Falge, E., Baldocchi, D., Papale, D., Aubinet, M., Berbigier, P., Bernhofer, C., Buchmann, N., Gilmanov, T., Granier, A., Grünwald, T., Havránková, K., Ilvesniemi, H., Janous, D., Knohl, A., Laurila, T., Lohila, A., Loustau, D., Matteucci, G., Meyers, T., Miglietta, F., Ourcival, J.-M., Pumpanen, J., Rambal, S., Rotenberg, E., Sanz, M., Tenhunen, J., Seufert, G., Vaccari, F., Vesala, T., Yakir, D., Valentini, R., 2005. On the separation of net ecosystem exchange into assimilation and ecosystem respiration: review and improved algorithm. *Glob. Change Biol.* 11 (9), 1424–1439. <http://dx.doi.org/10.1111/j.1365-2486.2005.01002.x/abstract>.
- Rogers, A., Medlyn, B.E., Dukes, J.S., Bonan, G., von Caemmerer, S., Dietze, M.C., Kattge, J., Leakey, A.D.B., Mercado, L.M., Niinemets, I., Prentice, I.C., Serbin, S.P., Sitch, S., Way, D.A., Zaehle, S., 2017. A roadmap for improving the representation of photosynthesis in earth system models. *New Phytol.* 213 (1), 22–42. <http://dx.doi.org/10.1111/nph.14283/abstract>.
- Running, S.W., Nemani, R.R., Heinsch, F.A., Zhao, M., Reeves, M., Hashimoto, H., 2004. A continuous satellite-derived measure of global terrestrial primary production. *BioScience* 54 (6), 547–560. <http://bioscience.oxfordjournals.org/content/54/6/547>.
- Ryan, M.G., 1990. Growth and maintenance respiration in stems of *Pinus contorta* and *Picea engelmannii*. *Can. J. Forest Res.* 20 (1), 48–57. <http://dx.doi.org/10.1139/x90-008#WPf7HGclHmg>.
- Sawada, Y., Tsutsumi, H., Koike, T., Rasmay, M., Seto, R., Fujii, H., 2016. A field verification of an algorithm for retrieving vegetation water content from passive microwave observations. *IEEE Trans. Geosci. Remote Sens.* 54 (4), 2082–2095.
- Scurlock, J.M.O., Johnson, K., Olson, R.J., 2002. Estimating net primary productivity from grassland biomass dynamics measurements. *Glob. Change Biol.* 8 (8), 736–753. <http://dx.doi.org/10.1046/j.1365-2486.2002.00512.x/full>.
- Suyker, A.E., Verma, S.B., Burba, G.G., Arkebauer, T.J., 2005. Gross primary production and ecosystem respiration of irrigated maize and irrigated soybean during a growing season. *Agric. Forest Meteorol.* 131 (3–4), 180–190. <http://www.sciencedirect.com/science/article/pii/S0168192305001127>.
- Tian, F., Brandt, M., Liu, Y.Y., Verger, A., Tagesson, T., Diouf, A.A., Rasmussen, K., Mbaw, C., Wang, Y., Fensholt, R., 2016. Remote sensing of vegetation dynamics in drylands: evaluating vegetation optical depth (VOD) using AVHRR NDVI and in situ green biomass data over West African Sahel. *Remote Sens. Environ.* 177, 265–276. <http://linkinghub.elsevier.com/retrieve/pii/S0034425716300852>.
- Tramontana, G., Jung, M., Schwalm, C.R., Ichii, K., Camps-Valls, G., Ráduly, B., Reichstein, M., Arain, M.A., Cescatti, A., Kiely, G., Merbold, L., Serrano-Ortiz, P., Sickert, S., Wolf, S., Papale, D., 2016. Predicting carbon dioxide and energy fluxes across global FLUXNET sites with regression algorithms. *Biogeosciences* 13 (14), 4291–4313. <http://www.biogeosciences.net/13/4291/2016/bg-13-4291-2016-metrics.html>.
- USGS, 1996. Global 30-Arc-Second Elevation Data Set (GTOPO30). <http://lpdaac.usgs.gov>.
- van der Schalie, R., de Jeu, R.A.M., Kerr, Y.H., Wigneron, J.P., Rodríguez-Fernández, N.J., Al-Yaari, A., Parinussa, R.M., Mecklenburg, S., Drusch, M., 2017. The merging of radiative transfer based surface soil moisture data from SMOS and AMSR-E. *Remote Sens. Environ.* 189, 180–193. <http://www.sciencedirect.com/science/article/pii/S0034425716304734>.
- van der Schalie, R., Kerr, Y.H., Wigneron, J.P., Rodríguez-Fernández, N.J., Al-Yaari, A., Jeu, R.A.M.d., 2016. Global SMOS Soil moisture retrievals from the land parameter retrieval model. *Int. J. Appl. Earth Observ. Geoinf.* 45B, 125–134. <http://www.sciencedirect.com/science/article/pii/S0303243415300179>.
- Verbesselt, J., Umlauf, M., Hirota, M., Holmgren, M., Van Nes, E.H., Herold, M., Zeileis, A., Scheffer, M., 2016. Remotely sensed resilience of tropical forests. *Nat. Clim. Change* 6 (11), 1028–1031. <http://dx.doi.org/10.1038/nclimate3108>.
- Vreugdenhil, M., Dorigo, W.A., Wagner, W., Jeu, R.A.M.d., Hahn, D., Marle, M.J.E.v., 2016a. Analyzing the vegetation parameterization in the TU-Wien ASCAT soil moisture retrieval. *IEEE Trans. Geosci. Remote Sens.* 54 (6), 3513–3531. <http://ieeexplore.ieee.org/articleDetails.jsp?arnumber=7410033>.
- Vreugdenhil, M., Hahn, S., Melzer, T., Bauer-Marschallinger, B., Reimer, C., Dorigo, W.A., Wagner, W., 2016b. Assessing vegetation dynamics over Mainland Australia With Metop ASCAT. *IEEE J. Select. Top. Appl. Earth Observ. Remote Sens.* PP (99), 1–9.
- Wagner, F., Rossi, V., Stahl, C., Bonal, D., Héroult, B., 2013a. Asynchronism in leaf and wood production in tropical forests: a study combining satellite and ground-based measurements. *Biogeosciences* 10 (11), 7307–7321. <http://dx.doi.org/10.5194/bg-10-7307-2013>.
- Wagner, W., Hahn, S., Kidd, R., Melzer, T., Bartalis, Z., Hasenauer, S., Figa-Saldaña, J., de Rosnay, P., Jann, A., Schneider, S., Komma, J., Kubu, G., Brugger, K., Aubrecht, C., Züger, J., Gangkofner, U., Kienberger, S., Brocca, L., Wang, Y., Blöschl, G., Eitzinger, J., Steinnocher, K., Zeil, P., Rubel, F., 2013b. The ASCAT soil moisture product: a review of its specifications, validation results, and emerging applications. *Meteorol. Z.* 22 (1), 5–33.
- Waring, R.H., Landsberg, J.J., Williams, M., 1998. Net primary production of forests: a constant fraction of gross primary production? *Tree Physiol.* 18 (2), 129–134. <http://treephys.oxfordjournals.org/content/18/2/129>.
- Woodhouse, I.H., 2005. *Introduction to Microwave Remote Sensing*. CRC Press.
- Wright, S.J., van Schaik, C.P., 1994. Light and the phenology of tropical trees. *Am. Nat.* 143 (1), 192–199. [http://www.jstor.org/stable/2462858?seq=1#page\\_scan\\_tab\\_contents](http://www.jstor.org/stable/2462858?seq=1#page_scan_tab_contents).
- Zhang, Y., Guanter, L., Berry, J.A., Tol, C.v.d., Joiner, J., 2016. Can we retrieve vegetation photosynthetic capacity parameter from solar-induced fluorescence? *IEEE International Geoscience and Remote Sensing Symposium (IGARSS)* 1711–1713.
- Zhao, M., Heinsch, F.A., Nemani, R.R., Running, S.W., 2005. Improvements of the MODIS terrestrial gross and net primary production global data set. *Remote Sens. Environ.* 95 (2), 144–176. <http://www.sciencedirect.com/science/article/pii/S0034425705000106>.
- Zribi, M., Chahbi, A., Shabou, M., Lili-Chabaane, Z., Duchemin, B., Baghdadi, N., Amri, R., Chehbouni, A., 2011. Soil surface moisture estimation over a semi-arid region using ENVISAT ASAR radar data for soil evaporation evaluation. *Hydrol. Earth Syst. Sci. Discuss.* 15 (1), 345–358. <http://hal.ird.fr/ird-00610514/document>.